Hydrodynamic characterization of continuous flow of Pickering droplets with solid nanoparticles in microchannel reactors

Wenxing Sun[a], Xunli Zhang[b], Chaoqun Yao[c], Qingqiang Wang[a], Nan Jin[a], Hongying Lv[a], Yuchao Zhao[a,*]

[a] Shandong Engineering Research Center of Green Manufacturing for New Chemical Materials, College of Chemistry & Chemical Engineering, Yantai University, Yantai 264005, China

[b] School of Engineering & Institute for Life Sciences, University of Southampton, Southampton SO17 1BJ, UK

[c] Dalian National Laboratory for Clean Energy, Dalian Institute of Chemical Physics, Chinese Academy of Sciences, Dalian 116023, China

Abstract

In this work, a method based on Pickering emulsion systems (PES) was proposed to manipulate multiphase processes containing solid particles in microchannels without adhesion and/or accumulation. The flow hydrodynamics of PES in a microchannel were systematically characterized. For comparison, a suspension system (SS, ethyl acetate with suspended SiO_2 nanoparticles-water) and a viscous fluid system (VFS, ethyl acetate with methyl-silicone oil-water) were examined. It was found liquid-liquid two-phase characteristics of PES, SS and VFS around T-junction within the main microchannel depended on surface hydrophobicity of stabilizing SiO_2 nanoparticles, amount of SiO_2 particles added, viscosity and flow rate. Four flow patterns were observed under these operating conditions for PES and VFS, where superficial velocity was the key factor affecting the flow patterns transition. Finally, a scaling law of the droplet size was established as a function of Q_d/Q_c, μ_d/μ_c and Ca.

Keywords: Microchannel reactors, Hydrodynamics, Pickering emulsion, Solid

* Corresponding Author. Tel: +86 535 6903386.
E-mail address: yczhao@ytu.edu.cn (Y. Zhao).

particles, Slug flow

1. Introduction

With the development of microchannel reactor technology for chemical process intensification and optimization, multiphase flow hydrodynamics, transport and reaction characteristics under microfluidic condition have received much attention and been intensively investigated over the past two decades (Jähnisch et al., 2004; Chen et al., 2006; Wang et al., 2013; Adamo et al., 2016; Jin et al., 2020). Compared with conventional macroscale reactors, the microreactor has demonstrated many advantages such as large specific interfacial area, fast heat and mass transfer rate, improved safety and controllability, and reduced backmixing. At present, the vast majority of work on multiphase systems in microreactors has been focused on gas-liquid and liquid-liquid processes, but limited work has been performed on continuous microfluidics for transporting solid particles across microchannel networks (Xu et al., 2008; Kim and Yoo, 2012; Zaloha et al., 2012; Abadie et al., 2013; Liedtke et al., 2013; Zhao et al., 2013; Yao et al., 2018). This is largely associated with (i) the characteristic microchannel geometry, (ii) the large surface area/volume ratio of microchannels, and (iii) the large surface energy of solid micro/nano particles. Consequently, those factors can result in clogging of microchannels by mechanical obstruction and/or adhesion of solid particles to microchannel surfaces, leading to unstable or uncontrollable flow and mass transfer processes. In view of the significance of heterogeneous chemical processes in the chemical industry, especially heterogeneous catalytic reactions involving solid catalyst particles, there is a

tremendous need to address the above challenges in order to effectively facilitate heterogeneous catalysis in microchannel reactors (Munirathinam et al., 2015; Tanimu et al., 2017; Yue., 2017).

To investigate microfluidic multiphase processes involving gas-liquid flow through microchannels filled with solid catalyst particles, Márquez et al. (2019) designed a series of micro-packed beds of solid particles and pillars. The gas-liquid two-phase flow hydrodynamics and the corresponding mass transfer rate were characterized by varying gas/liquid flow rates and the distance between pillars, together with the liquid hold-up and gas-liquid interfacial area. In another micro-packed bed reactor, Tidona et al. (2012) elucidated the liquid-to-particle mass transfer characteristics with a copper dissolution method by adjusting the ratio of hydraulic to particle diameter and the channel geometries. They demonstrated the enhancement of the gas-liquid-solid three-phase mass transfer performance and the heterogeneous reaction rate, which were attributed to the existence of the fixed catalyst particles. Along with those developments, however, there still remain some technical issues for the practical application of such micro-packed bed reactors, in terms of difficult replacement of the solid catalyst, poor controllability of multiphase flow, and large pressure drop.

Accordingly, a micro-suspended reactor configuration has been proposed. Liedtke et al.(2013, 2015) developed a micro-suspended reactor where solid catalyst particles were suspended in the fluid under Taylor flow, for the catalytic hydrogenation of methyl pentanol. However, the suspended solid particles were found to cause some significant problems including poor flow stability, frequent clogging of channels

when the solid catalyst suspension started to aggregate, and deposition of solid particles to the channel wall surface. Further, Kobayashi et al. (2004) developed a wall-coated microreactor with a very thin layer of catalyst particles coated onto the inner wall of microchannel, for conducting gas-liquid-solid hydrogenation reactions achieving a high conversion. Although the wall-coated microreactor had advantages in eliminating clogging and also reducing pressure drop, it suffered from some inherent drawbacks, such as low catalyst loading per unit volume, catalyst loss, and difficulties in refreshing or replacing the deactivated catalyst.

In recent years, the introduction of the Pickering emulsion into microchannel reactors has opened up new avenues for manipulating and controlling multiphase flow systems, in particular, to address the above mentioned challenges associated with involvement of solid particles in microchannel reactors (Liu et al., 2017; Vis et al., 2020). Differing from the traditional emulsion, the Pickering emulsion is stabilized by micro/nano solid particles (instead of liquid surfactants) with selected hydrophilicity or hydrophobicity, that help eliminate operating difficulties associated with traditional surfactants, such as the formation of foaming, difficulty in emulsifier separation, and product contamination. The Pickering emulsion has also a unique interface self-assembly property for micro/nano particles, reducing the possibility of collision and coalescence between the adjacent emulsion droplets (Leclercq et al., 2012; Yang et al., 2015). Furthermore, it is a thermodynamically stable system (Aveyard et al., 2003) with insignificant influence by the environmental conditions such as temperature and salt ion concentration. Most importantly, the surface energy of

micro/nano particles is released at the interface of liquid-solid, reducing the possibility of their adherence to the channel wall and their aggregation towards consequent clogging. When these micro/nano particles are functionalized as solid catalysts, droplet-based heterogeneous catalytic systems are formed having large liquid-solid two-phase interface and significantly reduced internal diffusion resistance (Shen et al., 2009; Crossley et al., 2010; Yang et al., 2010; Wang et al., 2012). Thus, the Pickering emulsion systems have been applied to oxidation, hydrogenation, condensation and enzyme catalysis for gas-liquid or liquid-liquid two-phase systems, due to their ultra-stable and large interface, biological compatibility and environmental friendliness (Zhang et al., 2016; Qi et al., 2018; Chang et al., 2021). Factually, the application of Pickering emulsion in heterogeneous catalytic reaction is still in the preliminary stage, and its prospects are worthy of being further investigated and explored. Recently, Vis et al. (2020) reported the first use of a tube-in-tube co-flow microfluidic approach for flow Pickering emulsion catalysis, which showed a nine-fold improvement in yield compared to the simple biphasic flow system offering a versatile new extension of Pickering emulsion catalysis. Nevertheless, to realize the full potential of the Pickering emulsion for applications in microchannel reactors it is essential to gain a fundamental understanding of the multiphase flow characterization involving solid particles within microreactors, which is lacking at present, however.

Built on our previous research on a Pickering emulsion-water system (PES) stabilized by SiO_2 nanopartricles with tunable surface properties (Meng et al., 2020), the present study aimed to systematically characterize the microfluidic behavior and

hydrodynamics of Pickering emulsions within microreactors under a range of operating conditions. For comparing with the PES, a suspension system (SS) formed with ethyl acetate containing suspended SiO_2 nanoparticles and water, and a viscous fluid system (VFS) consisting of ethyl acetate, methyl-silicone oil and water, were employed. A qualitative force analysis was carried out to gain insight into the mechanism of the flow pattern transition and the motion behavior of emulsion droplets. Furthermore, a dimensionless characteristic number L_D/w (i.e., length of dispersed phase droplet/width of microchannel) was investigated in order to establish a scaling law through empirical correlation.

2. Experimental section

SiO_2 nanoparticles (20 nm, Beijing Shenghe Haoyuan Technology Co., Ltd), methyltrimethoxysilane (Aladdin, CAS 1185-55-3) and ethyl acetate-water system (Sinopharm Chemical Reagent Co., Ltd, CAS 141-78-6) were chosen to prepare the stable Pickering emulsion according to our previous studies (Meng et al., 2020). In a typical process of surface modification of SiO_2 particles, raw SiO_2 particles (1.0 g), methyltrimethoxysilane (with selected amount) and toluene (30 mL) were successively added into the reactor vessels (100 mL) made of stainless steel. The six vessels in the unit contained either the same mixture for increasing production, or different ones for examining multiple parameters. The rotating unit, placed in a forced convection oven (KLJX-8a, Yantai Branch Chemical Equipment Co., Ltd) set at 130 ^oC, operated at an optimized rotating rate of 10 Hz for 12 h. The silanol group on the surface of SiO_2 particles underwent condensation reaction with the silane coupling

agent, with the increase of the amount of silane coupling agent, more hydrophobic groups were grafted on the surface of particles, so that the hydrophobicity became stronger. The surface of SiO_2 nanoparticles were modified to reduce its hydrophilicity by the surface grafting method with different amounts of methyltrimethoxysilane, i.e. 0.5 mL, 0.8 mL and 1.0 mL, denoted as M0.5, M0.8 and M1.0, respectively. During the preparation of the emulsion, the oil-water volumetric ratio of ethyl acetate to water was fixed at 7:5 and the amount of modified SiO_2 particles (0.25 g, 0.5 g and 0.75 g) was adjusted to prepare the W/O (water/oil) Pickering emulsions with different viscosity. Pickering emulsion exhibited great stability, it was found that droplets deposited at the oil phase bottom, but the droplet size did not change significantly after standing for 24 hours. The emulsions samples prepared were denoted as M0.5@S0.25, M0.5@S0.5, M0.5@S0.75, M0.8@S0.25, M0.8@S0.5, M0.8@S0.75, M1.0@S0.25, M1.0@S0.5, M1.0@S0.75, as shown in Table 1.

The contact angle of the Pickering emulsion was measured by an optical tensiometer (JC2000, Shanghai Zhongchen Digital Technology Equipment Co., Ltd) to quantify the hydrophobicity or hydrophilicity of the modified particle surface. The viscosity of Pickering emulsion was measured by a rotational viscometer (Brookfield DV2T, USA) at 24 ^{o}C. The interfacial tension between the continuous phase (water) and the dispersed phase (the Pickering emulsion) was measured by an interfacial tensiometer (DataPhysics OCA 15EC, Germany). The uncertainty of measurement was less than ±5%. Table 1 summarizes these measured physical properties of the three multiphase systems, namely, PES, SS and VFS, in terms of viscosity, interfacial

tension and droplet diameter.

Table 1. Physical properties of PES, SS and VFS

Testing system (24 ºC)		Viscosity μ(mPa·s)	Interfacial tension γ (mN/m)	Droplet diameter d (μm)
PES	M0.5@S0.25	3.39	7.64	171.88
	M0.5@S0.5	5.47	7.15	55.21
	M0.5@S0.75	10.21	7.00	41.67
	M0.8@S0.25	3.57	7.24	122.19
	M0.8@S0.5	5.84	6.92	50.45
	M0.8@S0.75	10.50	6.68	33.85
	M1.0@S0.25	4.03	7.31	103.44
	M1.0@S0.5	6.45	6.91	46.65
	M1.0@S0.75	10.94	6.79	27.97
SS	M0.5@S0.25	1.21	*	*
	M0.5@S0.5	1.38	*	*
	M0.5@S0.75	1.54	*	*
	M0.8@S0.25	1.29	*	*
	M0.8@S0.5	1.40	*	*
	M0.8@S0.75	1.54	*	*
	M1.0@S0.25	1.36	*	*
	M1.0@S0.5	1.47	*	*
	M1.0@S0.75	1.68	*	*
VFS		3.36	5.94	*
		5.38	6.36	*
		10.08	6.61	*
		3.55	7.56	*
		5.86	8.23	*
		10.59	8.46	*
		4.00	6.57	*
		6.40	7.30	*
		10.97	9.38	*

During the preparation of the Pickering emulsion, firstly, with the assistance of ultrasound (SB 3200D, Ningbo Xinzhi Biotechnology Co., Ltd), a selected amount of SiO_2 particles was dispersed in ethyl acetate at 20 kHz for about 5 min. Then, the deionized water was added into the ethyl acetate phase containing SiO_2 particles, which was mixed vigorously with a vortex mixer (IKA T25 digital Ultra Turrax, S25N-18G, German), set at a speed of 13,500 rpm for about 4 min. Finally, the obtained W/O Pickering emulsion was analyzed to characterize their morphology and

microstructure through visualization using an inverted microscope (Olympus IX73P2F, Japan) equipped with a 20× magnification of and a high speed digital camera (Phantom Miro R311, USA).

The suspension solution was prepared by mixing the same amount of modified SiO_2 particles with ethyl acetate assisted by ultrasound. The comparison of the Pickering emulsion and the suspension solution was carried out to validate the stability and the feasibility of the PES. The PES was also regarded as three-phase system, which included the modified SiO_2 particles, deionized water and ethyl acetate. A small amount of Sudan III was added into the emulsion phase to enhance visualization.

The experimental setup is schematically depicted in Fig. 1(a). The microchannel chip is a rectangle of 50 mm × 60 mm, the full-length of main channel is 167 mm, the cross section of the channel is an approximate square shape of 0.3 mm × 0.3 mm. The immiscible liquid-liquid two-phase fluids were introduced into the horizontal T-junction microchannel by two syringe pumps (Harvard 11 ELITE Single, USA) equipped with 10 mL syringes, respectively. A stereo microscope (Olympuss ZX2-ILLK, Japan) and a high speed digital camera (Phantom Miro R311, USA) were used to visualize two-phase flow patterns. The frame rates were set in the range of 3,200~10,000 fps (frames per second).

Fig. 1(b)&(c) illustrates the structure design and geometry of the microchannel reactor, where the continuous phase and the dispersed phase entered into two inlets, respectively. The microchannel reactor was made of quartz glass and sealed by a

thermal bonding method, fabricated by Suzhou Paifimeng Trading GmbH. Because of the strong hydrophilicity of the glass, the microchannel reactor was saturated initially with deionized water. During experiments, the volumetric flow rates of the dispersed phase and the continuous phase were set in the range of $10<Q_d<200$ μL/min and $10<Q_c<1300$ μL/min, respectively. The flow patterns were monitored at the T-junction regions with recorded snapshots and videos. The slug/droplet length was measured and averaged from at least 10 snapshots. In this work, *Re* and *Ca* for the continuous phase were in the ranges of 0.608~114.85 and 8.0×10^{-5}~0.05, respectively. After each experiment, the microchannels were cleaned by injecting acetone, acetic acid, and deionized water to remove residual chemicals, and finally dried ready for the next experiment.

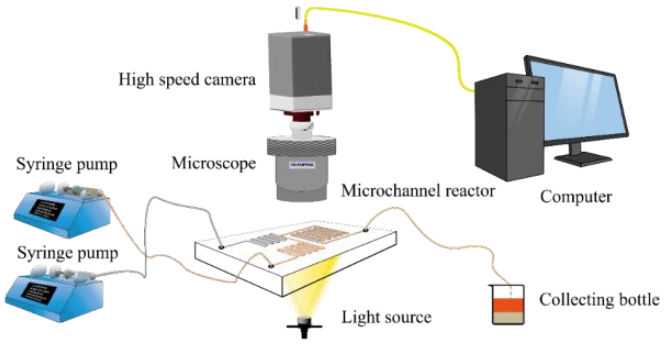

(a)

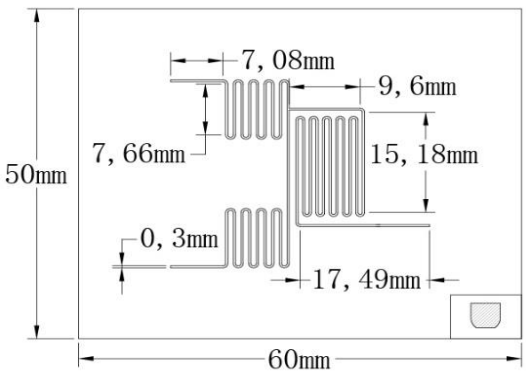

(b)

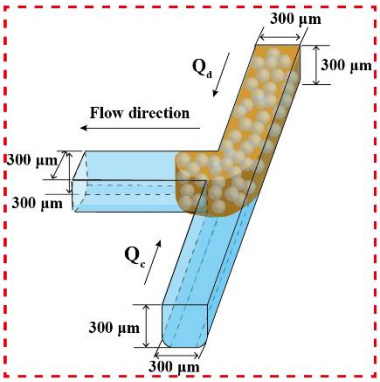

(c)

Fig. 1. (a) Schematic of experimental setup; (b) Layout design of microchannel reactor; (c) Schematic of the microchannel T-junction, 300 μm × 300 μm

3. Results and discussion

3.1 Characterization of the Pickering emulsions

The hydrophobicity of the surface of the modified SiO_2 nanoparticles was characterized by measuring contact angles of water droplets on the film coated with SiO_2 nanoparticles. The measurements (Fig. 2) showed that the contact angles increased from 18° of raw particles (M0.0) to 101° (M0.5), 127° (M0.8) and 143.3° (M1.0) as modified by a silane coupling agent methyltrimethoxysilane, respectively. As the amount of the silane coupling agent increased, the surface properties of SiO_2 nanoparticles switched from hydrophilicity to hydrophobicity, allowing to facilitate the formation of the W/O Pickering emulsion (Meng et al., 2020).

(a) (b) (c) (d)

Fig. 2. Contact angles of (a) raw (M0.0) and modified SiO_2 nanoparticles (dia. 20 nm) of (b) M0.5, (c) M0.8 and (d) M1.0

To examine the effect of the addition of SiO_2 nanoparticles on the emulsion droplet diameter, different amount of the modified SiO_2 nanoparticles with varying hydrophobicity were used. The results are shown in Fig. 3 and Table 1. As can be seen, increasing amount of SiO_2 nanoparticles resulted in reduction of the diameter of the dispersed droplets, but enhancement of the stability. For this system, the increase in SiO_2 nanoparticles amount improved the surface coverage, which decreased the

formed emulsion droplet size. This was likely due to the formation of a 3D network structure around the emulsion droplets that enhanced the stability of the Pickering emulsion (Binks et al., 2010). Binks' group (Aveyard et al., 2003) systematically studied the influence of SiO_2 particles concentration on the droplet size of Pickering emulsion system. They found that in a low particle concentration range (lower than 3%), the droplet size of the emulsion would decrease with increasing particle concentration. In this work, the concentration of SiO_2 particles is in the range of 2-6%. A 10-fold increase in particle concentration reduced the droplet size to about 1/8 of the original. That was overall well in line with the previous observation (Binks et al., 2004, 2005; Liu et al., 2012).

When the concentration of particles was higher than 3%, the droplet size would not change with the increase in particle concentration, and the extra particles tended to disperse in the continuous phase, not adsorb at the droplet interface. The stabilization mechanism is that the increase of the addition amount of solid particles means that the increase of the number of solid particles adsorbed at the oil-water interface, which leads to the thickening of the interface film, the enhancement of the ability to prevent the coalescence between droplets. In addition, coalescence is inhibited by the excess of particles because they enter oil phase and form a three-dimensional network, which increases the distance between droplets and stability (Binks et al., 2010).

As the amount of particles adsorbed on the oil-water interface increased, the oil-water interfacial tension decreased while a dense interface film formed, which effectively prevented the collision and the coalescence between the emulsion droplets.

Although the hydrophobicity of SiO_2 was in favor of the formation of the W/O Pickering emulsions, it had insignificant effect on the diameter of the droplets, that may be associated with a combination of a number of factors such as the non-spherical structure, the size distribution and the surface roughness of SiO_2 particles (Binks et al., 2000; Binks et al., 2005; Wu and Ma, 2016) (Fig. 3).

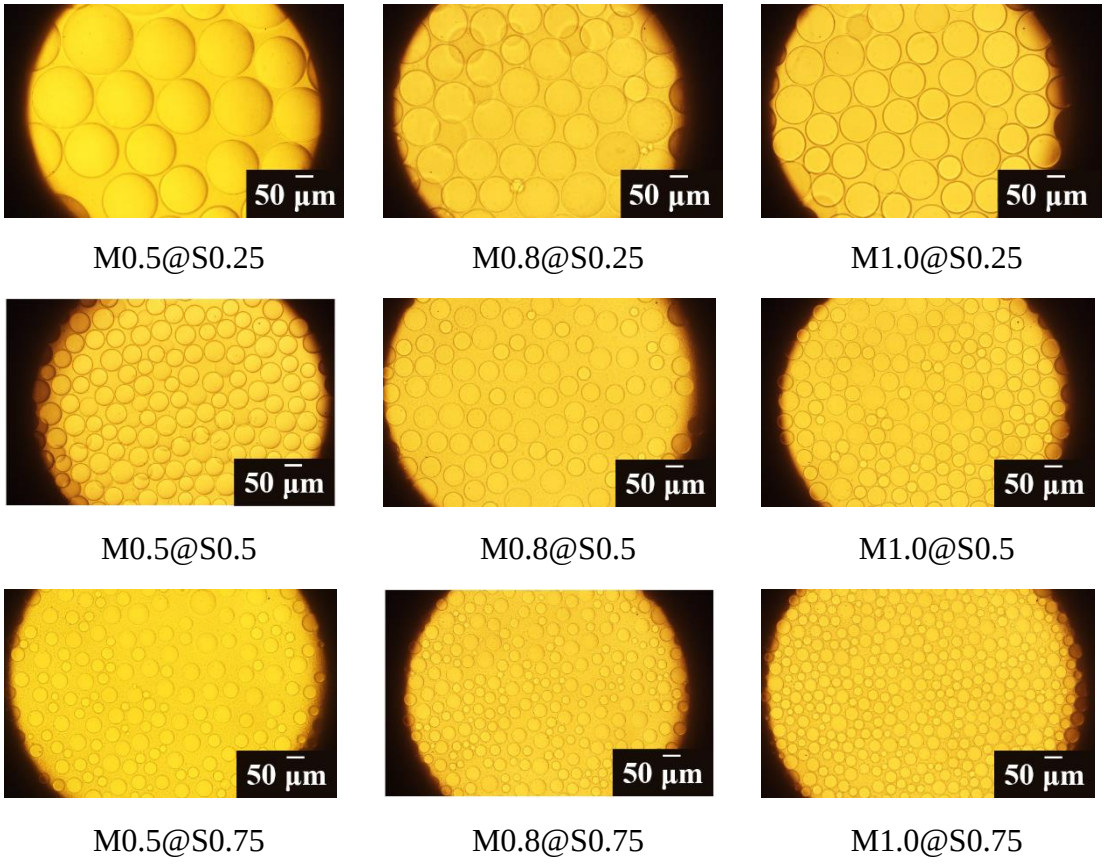

Fig. 3. Microscope image of Pickering emulsion droplets

3.2 Two-phase flow patterns of three systems of PES, SS and VFS

When the PES contains high-solid content and dispersed emulsion droplets, the apparent viscosity and density are generally high, exhibiting similar characteristics to fluids having high viscosity (Yao et al., 2018; Archibong-Eso et al., 2019; Wang et al., 2021). In order to identify the suitable operational parameters for achieving stable Pickering emulsion flow within microchannels, the prepared three multiphase flow

systems, i.e. PES, SS and VFS, were examined and compared. It is worth to note that the high viscous fluid was used as the dispersed phase in those three systems, which has been less studied previously (Cubaud and Mason, 2008; Bai et al., 2016; Zhang et al., 2019).

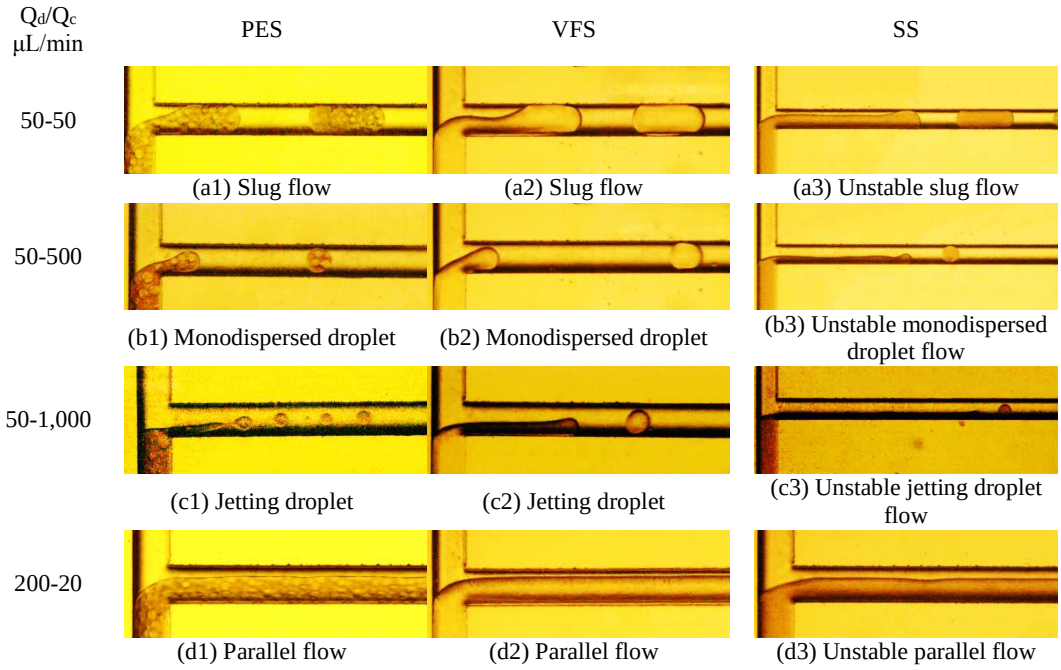

Fig. 4. Flow patterns observed around T-junction for three systems of PEs, SS and VFS

Fig. 4 illustrates the observed flow patterns with images covering the microchannel section across 20 mm downstream of the T-junction to allow the flow to fully develop. Four categories of stable flow patterns were observed for PES and VFS having comparable viscosities, namely, slug flow, monodispersed droplet flow, jetting droplet flow and parallel flow (Fig. 4). In these systems, the demulsification phenomena of Pickering emulsion in microchannel were not observed in all experiments. However, liquid-liquid two-phase immiscible flow patterns for SS were unstable, where the solid content of SS was identical with that of PES. These were similar to the previous observations, e.g. during the formation of other viscous droplets (Cubaud and Mason,

2008). In general, the formation of any specific flow pattern is a combination of many factors in the complex multiphase system under dynamic fluidic conditions, including fluid properties, fluidic operating parameters, and microchannel geometry/surface properties. The forces involved during the formation of dispersed droplets are further analyzed in the next Section.

For SS, the aqueous phase in the dispersed Pickering emulsion phase was replaced by ethyl acetate with the same volume. Fig. 5(a) shows that the suspension stretched along and attached to the channel wall when leaving the T-junction. Therefore, it was difficult to cut off the neck of the dispersed suspension phase at the T-junction. Fig. 5(b) shows that the dispersed droplets were formed at around the first bend of the main channel after flowing over a longer distance along the flow direction compared to PES, which was largely induced by Rayleigh-Taylor instability (Vadivukkarasan, et al., 2020). However, the dispersed droplets still tended to attach to the channel wall, which made the interface being elongated and deformed, even blocking the channel and finally forming some unstable flow patterns, as shown in Fig. 5(c).

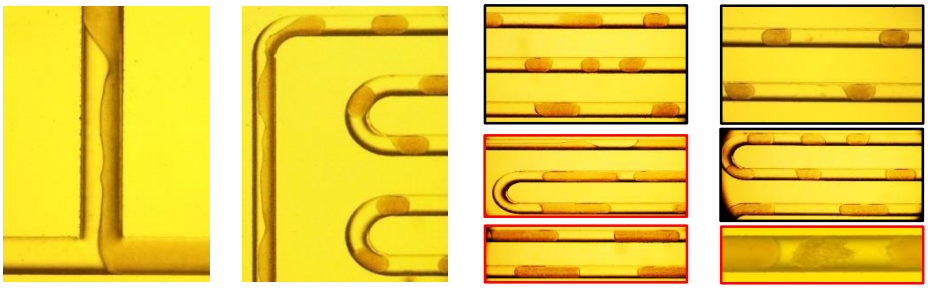

Fig. 5. Flow patterns of SS at different positions in microchannel (a) Around T-junction; (b) Around the bends of the microchannel; (c) In the main microchannel

For VFS, silicone oil was used to regulate the viscosity of ethyl acetate (oil phase),

in order to obtain comparable viscosities to that of the Pickering emulsion. The flow patterns and their formation processes are shown in Fig. 6. Four distinct flow patterns were also observed similar to that of PES, i.e. slug flow, monodispersed droplet flow, jetting droplet flow and parallel flow. These flow patterns were mainly formed by squeezing, dripping and jetting regimes, in accordance with observations in previous investigation with VFS by Yao et al. (2018) and Bai et al. (2016). In this work, the viscosity of PES increased with the increase in the addition amount of SiO_2 nanoparticles. In order to further clarify the influence of the dispersed W/S/O spherical emulsion droplets ($Ph_{2\text{-}1}$) on the formation of the dispersed Pickering emulsion phase, the introduction of VFS as a benchmark with the same viscosity should be important and necessary. For avoiding redundancy of the description about well known VFS, we tried our best to only list part experimental results. As VFS was out of the main scope of the present work, more experimental results for VFS are shown in Supporting Information.

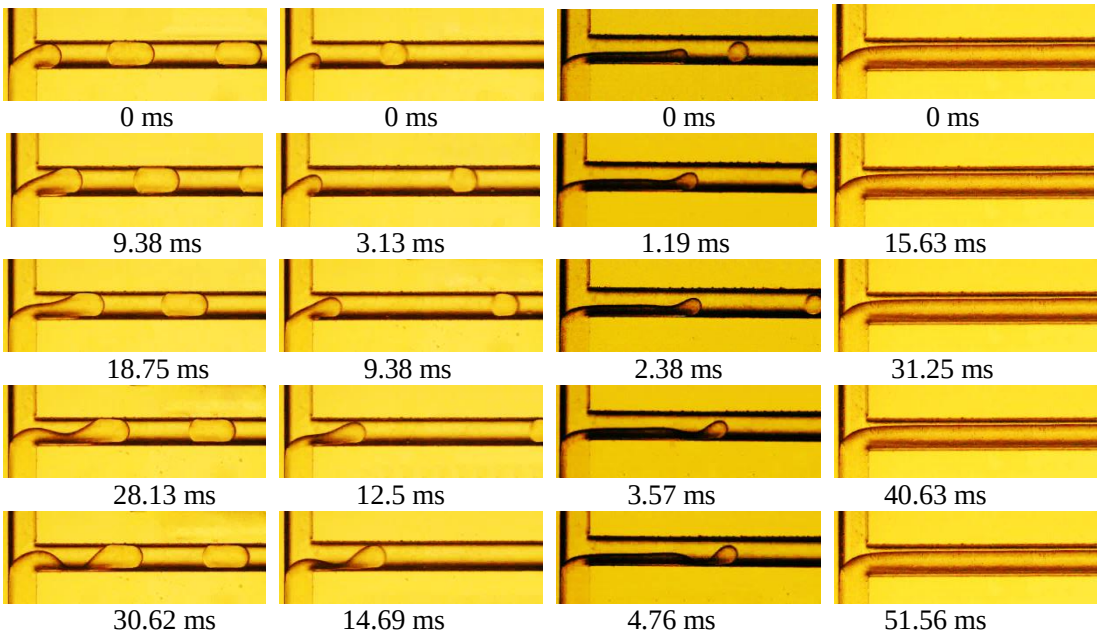

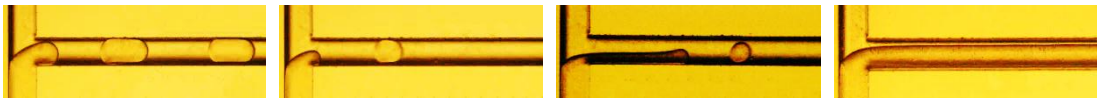

34.06 ms (a) 16.25 ms (b) 6.43 ms (c) 54.69 ms (d)

Fig. 6. Flow patterns and their formation processes for VFS. (a) Squeezing: Q_d=50 μL/min, Q_c=100 μL/min. (b) Dripping: Q_d=50 μL/min, Q_c=500 μL/min. (c) Jetting: Q_d=50 μL/min, Q_c=1000 μL/min. (d) Laminar: Q_d=200 μL/min, Q_c=20 μL/min

The above observed different flow patterns may have different effects on potential reaction applications involving Pickering emulsion, where both well-defined contact interface and the recirculation within the continuous phase or the dispersed phase exist. The former is conducive to the regulation of the reaction processes. The latter can significantly enhance local mixing leading to augmented heat and mass transfer (i) in the radial direction within the liquid slug, and (ii) in the axial dispersion across the gas-liquid interface, which is similar to the issues of gas-liquid two-phase systems (Kececi et al. 2009; Su et al. 2012). Therefore, Slug flow and Monodispersed droplet flow are believed to be more favourable for potential reaction applications.

3.3 Formation mechanism of PES dispersed droplets in microchannel

As discussed above, the PES was composed of a continuous water phase (Ph_1) and a dispersed Pickering emulsion phase (Ph_2), where the formation of the dispersed droplets was the result of a number of forces exerted upon the emerging droplet (Pickering emulsion). Fig. 7 illustrates those forces, including the inertia force caused by Ph_1 ($F_c \propto d_H^2 u_{WS}^2 \rho_W$) and by Ph_2 ($F_d \propto d_H^2 u_{PS}^2 \rho_P$), the interfacial force at the neck of Ph_2 ($F_\gamma \propto \gamma_{W/P} \delta_{neck}$), the viscous shearing force ($F_\mu \propto \mu_W Q_W L_D / \delta_{gap}^2$) caused by the flow of Ph_1 around the emerging droplet, the continuous phase pressure on the neck

(P_{neck}) and the tip (P_{tip}) of Ph_2 (Fig. 7).

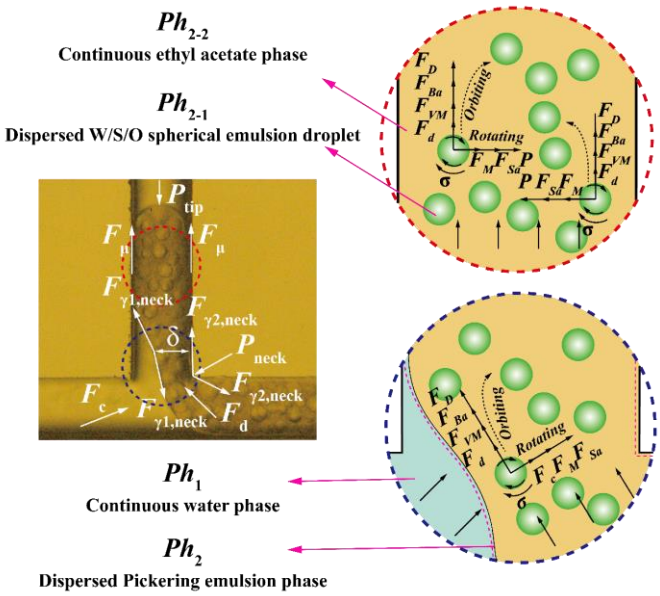

Fig. 7. Correlative forces for the formation of the dispersed droplets

The formation of the dispersed droplets was also believed to be the result of the dynamic competition among these forces. Specifically, as shown in Fig. 7, F_c and F_d were the main forces to drive Ph_2 to the downstream of the channel. F_μ also promoted the tip of Ph_2 towards the downstream, and caused the neck of Ph_2 to be quickly cut off, accelerating the formation of droplets. In addition, F_γ played an important role on the balance and the stability of the emerging droplet. At the neck of the dispersed phase, F_γ was balanced with F_c, F_μ and P_{neck} to ensure the dispersed phase to flow downstream continuously. The interfacial force caused the tail of the next emerging droplet to retract as the dispersed droplet forms, and the flow got into the transiently stable state. The interfacial force at the tip of the emerging droplet was balanced with F_μ and P_{tip}, in addition to the environmental confinement in the case of microchannels, to keep it moving downstream.

On the other hand, the dispersed W/S/O spherical emulsion droplets ($Ph_{2\text{-}1}$) and the continuous ethyl acetate phase ($Ph_{2\text{-}2}$) formed Pickering emulsion, as shown in Fig. 7(b). $Ph_{2\text{-}1}$ may be considered as quasi-solid soft microspheres due to SiO_2 particles acting as solid surfactant, where its moving trail was determined commonly by the drag force ($F_D \propto C_D \rho_o \left(u_o - u_{Ph_{2\text{-}1}}\right)^2 A_{Ph_{2\text{-}1}}$) induced by a range of factors, including $Ph_{2\text{-}2}$, the interfacial tension at the S/O interface (σ), the confinement of the microchannel wall, Basset force (F_{Ba}), virtual mass force (F_{VM}), Magnus force (F_M), Saffman force (F_{Sa}), and the collision and the repulsion forces between the adjacent emulsion droplets. The formation of the dispersed droplets was affected by the motion of $Ph_{2\text{-}1}$ in Ph_2, which depended on the size of $Ph_{2\text{-}1}$. The diameter of the dispersed droplets could be controlled by changing the addition amount of SiO_2 nanoparticles, and the dispersed phase neck formed with small size of $Ph_{2\text{-}1}$ was narrow. In addition, the small size of $Ph_{2\text{-}1}$ had a smaller torque, which increased the particle rotation speed, reduced the parabolic radian of motion, weakened the effect of F_D, accelerated the contract of neck, and led to the decrease of the size of the dispersed droplet.

The motion behaviors of $Ph_{2\text{-}1}$ in Ph_2 can be characterized over two regions, i.e. at the T-junction and in the main microchannel, as shown in Fig. 7(a). As the tip of the emerging Ph_2 began to intrude into the main channel at the T-junction, torque of $Ph_{2\text{-}1}$ occured under the action of F_c , F_d and F_D. The rotating motion was verified by an approximate clockwise direction. $Ph_{2\text{-}1}$ moved to the center of the microchannel due to F_M and F_{Sa}. Generally, the motion trajectory was more complex at the vicinity of T-junction due to the location distribution of $Ph_{2\text{-}1}$. Once the tip intruded into the main

channel, the streamline of all $Ph_{2\text{-}1}$ was almost identical and their vector direction was the same with F_{μ}, the disappearance of the rotation of $Ph_{2\text{-}1}$, F_M and F_{Sa}, so flow field was close to be stable and the motion trajectory showd a straight line (Fig. 7(b)).

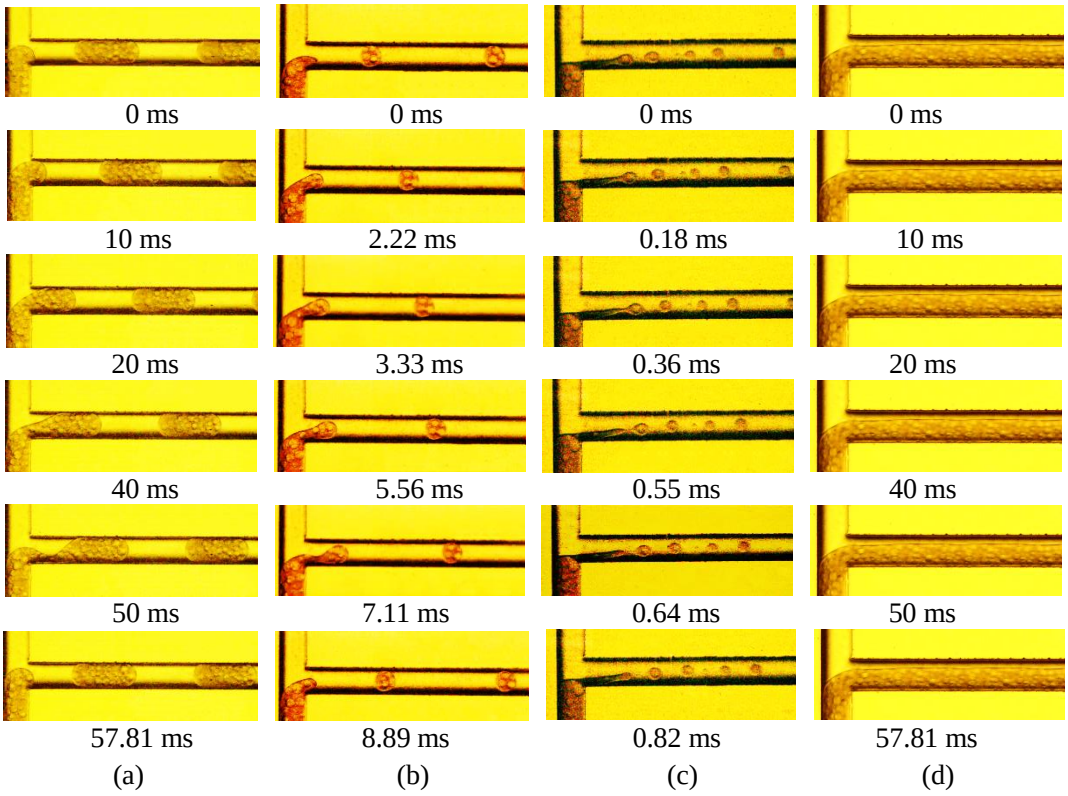

Fig. 8. Formation of the dispersed droplet for PES

(a) Squeezing, Q_d=50 μL/min, Q_c=50 μL/min; (b) Dripping, Q_d=50 μL/min, Q_c=500 μL/min; (c) Jetting, Q_d=50 μL/min, Q_c=1000 μL/min; (d) Laminar: Q_d=200 μL/min, Q_c=20 μL/min

Whilst the above analyzed forces affected the formation of Pickering emulsion droplets, they also influenced the overall multiphase flow behavior along the microchannel, forming different flow patterns under certain fluidic conditions (Fig. 4). Fig. 8 depicts the experimental observation captured during the formation of slug flow, monodispersed droplet flow and jetting droplet flow, by taking M1.0@S0.75 Pickering emulsion as an example, as detailed below.

Fig. 8(a) shows the dynamic formation of slug flow for PES at the T-junction in the

microchannel. The length of Pickering emulsion slugs was larger than the microchannel width. These slugs flowed along the channel, and were segmented from each other by the liquid plugs of Ph_1. Moreover, a thin continuous phase liquid film was located between the slug and the wall. This flow pattern was observed at a low Ph_1 flow rate (50 mL/min) and a 1:1 flow rate ratio of Ph_2 to Ph_1. In addition, the formation process of slug flow conformed to the squeezing mechanism. At the beginning of Ph_2 growth stage, the growth direction was perpendicular to the flow direction of the continuous phase in the main channel, and F_γ was dominant. Also, the size and the amount of $Ph_{2\text{-}1}$ had important influence on the formation and the width of the neck of the Ph_2 (Pan et al., 2018). Subsequently, Ph_2 gradually expanded at the inlet T-junction until blocking the main channel from time 0 ms to time 10 ms. The continuous phase flowed through the gap between Ph_2 and the channel wall, where the velocity of the continuous phase increased, as well as F_μ.

Fig. 9 schematically shows further analysis on the motion trajectory of $Ph_{2\text{-}1}$ in Ph_2, based on the observation captured by videos. It was found that $Ph_{2\text{-}1}$ on both sides of Ph_2 near the channel wall moved faster and migrated to the center of the channel (SI, Fig. S1). This was likely associated with $Ph_{2\text{-}1}$ around the tip tending to move clockwise as the torque induced the combined action of F_c, F_d and F_D. In the squeezing stage, the tip of Ph_2 continued to grow downstream under the balance with F_c, F_γ and P_{neck}, while the width of the neck of Pickering emulsion gradually decreased from time 10 ms to time 50 ms. At time 50 ms, the two-phase interface at the neck of the dispersed phase became a concave shape, which was similar to that of

high viscous fluid as the dispersed phase (Bai et al., 2016). Finally, the neck of the dispersed phase collapsed at time 52.81 ms. When the tail of the formed Pickering emulsion slug and the head of the new droplet quickly retracted due to the interfacial tension, the process entered into next squeezing period.

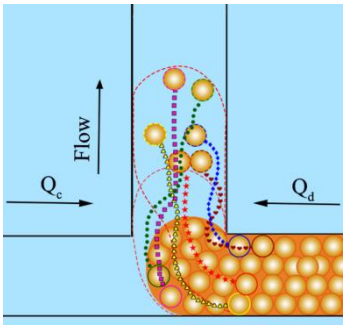

Fig. 9. Diagram of the motion trajectory of $Ph_{2\text{-}1}$ in Ph_2 (Q_c= Q_d=50 μL/min)

When the ratio of two-phase flow rate was relatively low (0.03~0.24), monodispersed drop flow and jetting droplet flow patterns were observed (Fig. 8 (b)&(c)), where higher continuous phase flow rates were favorable for forming jetting droplet flow. The formation of monodispersed droplets corresponded to the dripping mechanism. As the tip of the dispersed phase was unable to block the main channel due to the high continuous phase flow rate, it had to flow downstream under the strong push of F_μ and F_c. At the growth stage, the dispersed W/S/W/O spherical emulsion droplets entered into the tip of the dispersed phase, which expanded axially and radically, for example, from time 0 ms to time 3.33 ms. At the rupture stage, the neck of the dispersed phase began to gradually become narrower and slender, and only $Ph_{2\text{-}2}$ in Pickering emulsion can flow into the tip through the narrow neck, as seen from time 3.33 ms to time 8.89 ms in Fig. 8(b).

The length of the monodispersed droplet formed by the dripping mechanism was

smaller than the microchannel width because the shearing from the inertial or viscous force of the continuous phase was stronger than the two-phase interfacial tension. As the continuous phase flow rate continued to increase, Pickering emulsion phase was elongated and extended to downstream, thus the long narrow liquid column formed, which was pushed towards the center of the channel under the strong inertial force of the continuous phase (SI, Fig. S1). Due to the classical Rayleigh-Plateau instability (Xiao et al., 2016), the breakup of the tip of the Pickering emulsion occurred and small spherical droplets were formed at the moment of time 0.82 ms (Fig. 8(c)), i.e. the narrow liquid column was pinched off to form the jetting droplet flow.

When the flow rate ratio of dispersed phase to continuous phase was relatively high F_d began to dominate. As the dispersed phase cannot be cut off, it flowed side-by-side with the continuous phase in the microchannel (Fig. 8(d)). In this case, no dispersed droplets were formed, neither were slugs.

Overall, the diameter of Pickering emulsion droplets and the movement of $Ph_{2\text{-}1}$ were decisive factors for flow pattern and transition. With the decrease of SiO_2 amount, the diameter of emulsion droplets increased gradually, so δ was also relatively large that flow pattern transition needed larger j_c. When the diameter of the droplet was larger, the distribution became tighter, which led F_D increases on $Ph_{2\text{-}1}$, so the contraction of the neck of Ph_2 was inhibited, and the flow pattern transition lines were raised eventually.

3.4 Flow pattern maps for PES in microchannels

As discussed above, the formation of a specific flow pattern is determined by a

number of factors, including fluid properties and operating parameters, during the complex multiphase flow within a given microchannel. To identify suitable operating conditions in order to achieve a specific flow pattern, were varied the hydrophobicity of SiO_2 nanoparticles, the amount of SiO_2 nanoparticles added, and both phases' superficial flow velocities (j_d and j_c for dispersed and continuous phase, respectively). The properties and amounts of SiO_2 particles are specified in Table 1, while the two phases' superficial flow velocities, j_d and j_c, were operated in the range of j_d=0~40 mm/s and j_c=0~350 mm/s, respectively. Fig. 10 shows the flow pattern maps corresponding to those variables, with the transition curves dividing different flow pattern zones.

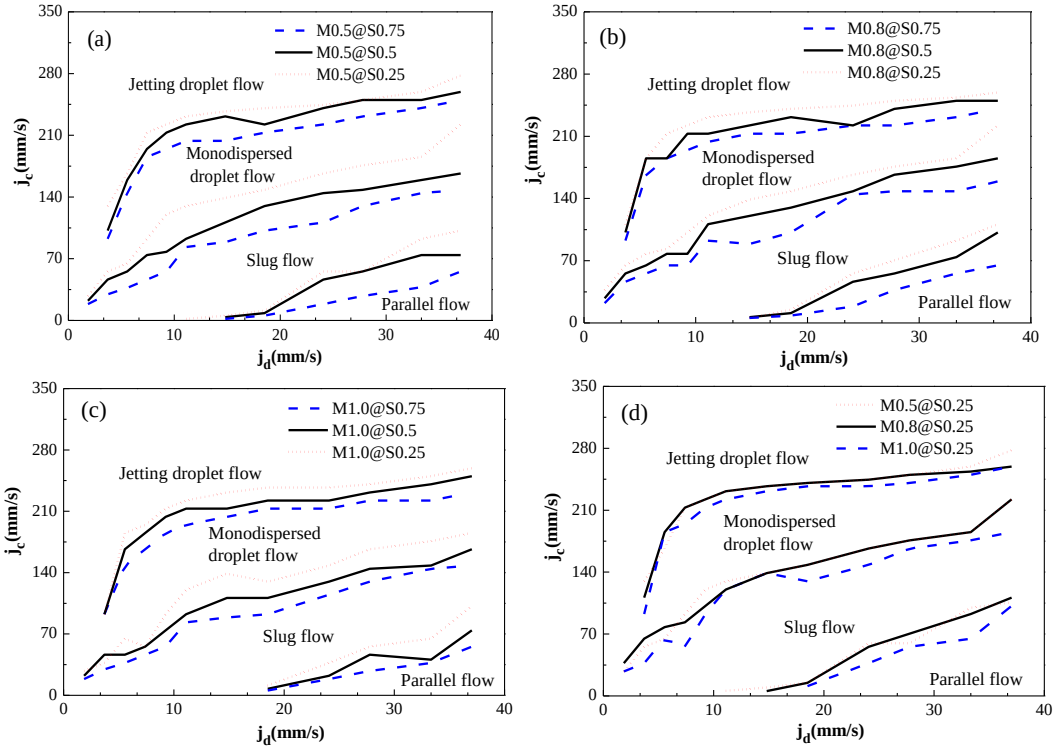

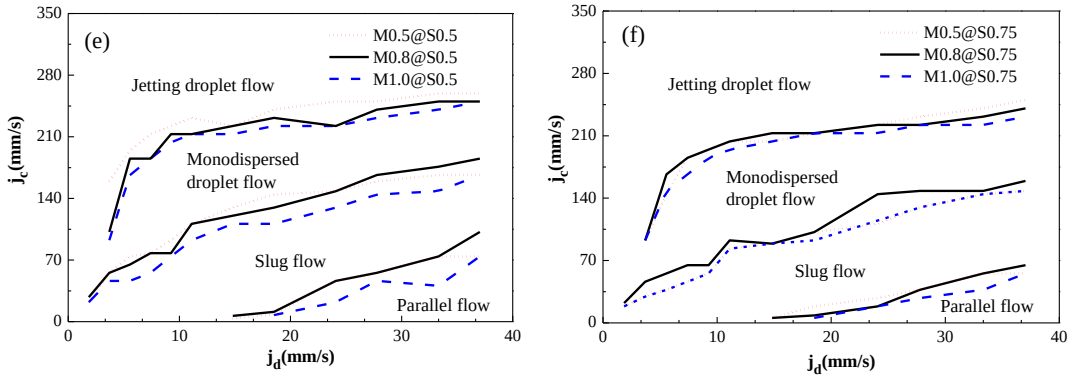

Fig. 10. Flow patterns and flow pattern transition lines for PES flow in microchannels with varying superficial velocities of dispersed phase and continuous phase, and amounts of methyltrimethoxysilane and SiO_2 nanoparticles

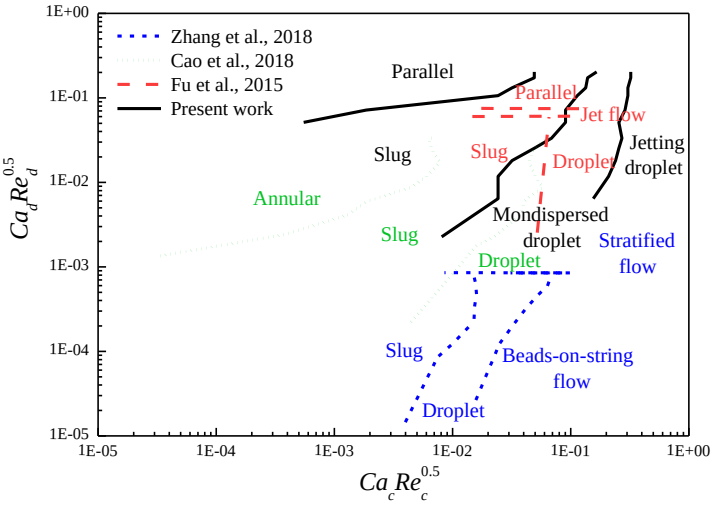

Fig.11. Comparison between the flow pattern map in the present study and that in the literature

As can be seen in Fig. 10(a), for a specific multiphase system increasing one phase's superficial velocity required to increase the other phase's velocity in order to realize a flow pattern transition. At a given j_d level, increasing j_c facilitated the transition from parallel flow, through slug flow and monodispersed drop flow, to jetting droplet flow. Clearly, the parallel flow zone occupies the smallest zone, located at the bottom right corner of the flow pattern map, requiring a higher flow rate ratio of Ph_2 to Ph_1 under high flow rates of Pickering emulsion. It was interesting to note that

those trends applied to all multiphase systems examined (Fig. 10(a)-(f)). Also, these observations were in line with that shown in Figs. 4 & 8.

For a given j_d, when increasing j_c, the flow pattern transited from parallel flow to stable slug flow, mainly due to the dominance of F_γ over F_c and F_μ. By further increasing j_c, the flow pattern changed from slug flow to monodispersed drop flow, finally to jetting droplet flow, while the shearing from large F_c or F_μ dominated over F_γ forming monodispersed drop flow and jetting droplet flow patterns. Compared to traditional liquid-liquid two-phase systems, the regions of the dispersed flow patterns (slug flow, monodispersed drop flow and jetting droplet flow) significantly increased (Zhao et al., 2006; Tsaoulidis et al., 2013; Cao et al., 2018; Yao et al., 2018). Also, the dispersed flow patterns easily formed with PES, which increased the feasibility of the solid conveying based on Pickering emulsion.

Regarding effect of added SiO_2 amount, Fig. 10(a)-(c) show that the decrease of SiO_2 amount, for a selected amount of methyltrimethoxysilane at a given j_d level, shifted upwards all the transitions curves requiring higher j_c, i.e. the smaller amount of SiO_2 added, the higher j_c, needed. This may be explained by the decrease of viscosity and two-phase interfacial tension, and the increase of diameter of the dispersed emulsion droplets in Pickering emulsion, given a decreased amount of SiO_2 nanoparticles added. During the formation of the dispersed emulsion droplet, the size of $Ph_{2\text{-}1}$ affected the break-up of the neck except for the balance between the shear stress and the interfacial tension according to our experimental observation. Moreover, the larger the $Ph_{2\text{-}1}$ size was, the stronger the impediment for the break-up of the neck

was. The effects of the amount of methyltrimethoxysilane, i.e., the hydrophobicity of SiO_2 nanoparticle surface on flow patterns are illustrated in Fig. 10(d)-(f), showing insignificant influence. This was mainly due to the variation of the Pickering emulsion droplet diameter to be insignificant with the increase of the methyltrimethoxysilane amount for a given amounts of SiO_2 nanoparticle, as shown in Figs. 3. For S0.25, with the increase of methyltrimethoxysilane amount, the critical velocity of Pickering emulsion for forming parallel flow gradually increased, which may be caused by the larger Pickering emulsion droplet diameter, as shown in Figs. 3 & 10(d). This was a typical situation where F_d or F_μ dominated over F_γ.

Fig. 11 shows the comparison between results from the present study and those in the literature. Based on the above discussion, key factors including viscosity, interfacial tension, two-phase velocity, characteristic scale of Pickering emulsion droplets and its motion of $Ph_{2\text{-}1}$ in Ph_2 all play an important role in the formation of the flow patterns, and further in the flow pattern transition boundary on the flow pattern map. Therefore, the composite dimensionless numbers were adopted to plot the flow pattern map, which were also employed previously (Yagodnitsyna et al., 2016; Yao et al., 2018).

As seen in the map, overall the central zone of the flow pattern map was occupied by the slug flow, which belonged to the interfacial tension dominated zone and the squeezing regime. The slug-droplet transition line in the present experiment shifted to top-left in the map compared to the traditional two-phase system (Cao et al., 2018; Zhang et al., 2018). This was attributed to larger interfacial tension and viscosity of the dispersed phase for PES, which postponed the occurrence of the dispersed droplets. Moreover, the trends of almost all the transition lines were similar. It indicated that the results from traditional high viscous systems could be extrapolated to PES in the microchannel.

By increasing the velocity or viscosity of the dispersed phase for traditional

systems, the parallel flow was prone to be formed under the domination of the dispersed inertia or viscous force. The viscosity of Ph_2 for PES increased with the increase in the solid content, whilst the diameter of $Ph_{2\text{-}1}$ reduced. Further, the neck width of the dispersed phase at the T-junction became narrower, which was unfavorable for the formation of the parallel flow. Other transition lines in the cyclohexane-CMC two-phase flow in rectangular microchannels were almost vertical (Fu et al., 2015), which were different from the present observation. That was likely due to the interfacial tension of their system being remarkably large (37 mN/m), which led to the increase of the interfacial tension dominated zone.

3.5 The length of the dispersed droplets in PES, SS and VFS

Upon establishment of a stable state for the formation of Pickering emulsion dispersed droplets, it is also important to characterize and, ultimately, achieve the desired droplet geometry. Within a confined microchannel, the dimensionless number L_D/w (i.e., length of dispersed phase droplet/width of microchannel) represents a characteristic quantity to describe the physical geometry of droplets under flow. Fig. 12(a)-(c) plot the variation of L_D/w as a function of total flow rate (Q_t) at a constant flow rate ratio of Q_d/Q_c = 1:1 for the PES flowing along the main microchannel. Different amounts of SiO_2 particles (0.25 g, 0.50 g and 0.75 g) with varying hydrophobicity (by adding 0.5 mL, 0.8 mL and 1.0 mL silane coupling agent) were employed. For comparison, an SS flow system was examined under the identical operating conditions (Fig. 12(d)-(f)). A wider range of operating conditions was also applied and the experimental results together with flow patterns observed are presented in Supporting Information (SI, Figs. S2-S3).

As can be seen in Fig. 12(a) for the PES, L_D/w decreased with the increase of total

two-phase flow rate for all three amounts SiO_2 addition, while the increase of modified SiO_2 addition resulted in the decrease in L_D/w. With the increase of SiO_2 amount, the diameter of emulsion droplet decreased, which was conducive to the contraction of the neck width of the dispersed phase (δ), and accelerated the droplet fracture under the same operating conditions. By increasing hydrophobicity following more silane coupling agent added from 0.5 mL to 1.0 mL (Fig. 12(a)-(c)), L_D/w was reduced correspondingly. As the two-phase interfacial tension almost kept constant with the increase of the amount of SiO_2, its effects on the the droplet length could be negligible. On the other hand, the increase of SiO_2 amount was in favor of the decrease of the neck width of the dispersed phase at the T-junction, potentially leading to decrease of the size of the emulsion droplet in Ph_2 and, in turn, decrease in L_D/w.

For the SS flow under identical operating conditions (Fig. 12(d)-(f)), it showed a similar trend in terms of L_D/w as a function of total flow rate, where L_D/w was generally larger than that of PES. More significantly, all SS flows appeared to be very unstable without obvious regularity, which was largely due to the adhesion of solid particles on the channel wall (Fig. 5). It was found that the solid particles in the suspension were easy to deposit at the bottom and adhere to the microchannel in SS, resulting in channel blockage. The solid particles in the suspension were easy to deposit under the action of gravity (F_G), which finally entered the water phase from the oil phase due to the drag force (F_D) produced by its own adhesion channel. This was a typical F_D dominated interfacial tension (F_γ).

Meanwhile, the comparison of the dispersed droplet length of VFS and PES is

depicted in Fig. 13. The experimental results showed that the length decreased with the increase of the dispersed phase viscosity for a given Q_d/Q_c, and it was in accordance with the literature reports (Bai et al., 2016). It was also found that the length for VFS was clearly larger than PES under the identical operating conditions, and the difference was induced by the emulsion droplet in Ph_2. The experimental results for other operating conditions are shown in SI, Fig. S4-S5.

On the one hand, there were little differences in both two-phase interfacial tension and viscosity between PES and VFS (Table 1), where their influence on the formation of the dispersed phase droplets was insignificant. With the increase of Ph_2 viscosity, meanwhile, the diameter of $Ph_{2\text{-}1}$ was smaller, which made the neck width of the dispersed phase decrease and F_μ become the dominant force, so the size of Ph_2 decreases. On the other hand, the existence of the emulsion droplets in Ph_2 promoted the break-up of the neck. Moreover, the smaller the diameter of the emulsion droplets was, the faster the collapsing velocity of the neck was. In order to elucidate the mechanism of the effects of the dispersed emulsion droplet in Ph_2, further study will be required, which is ongoing in our laboratory.

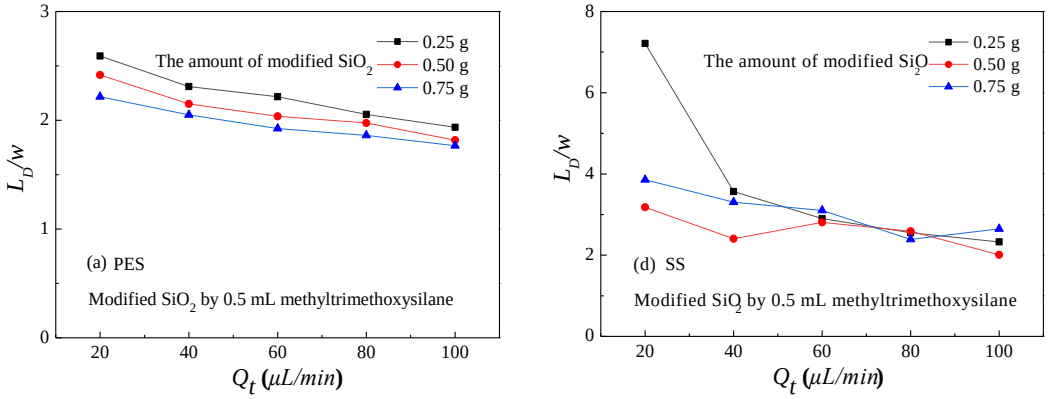

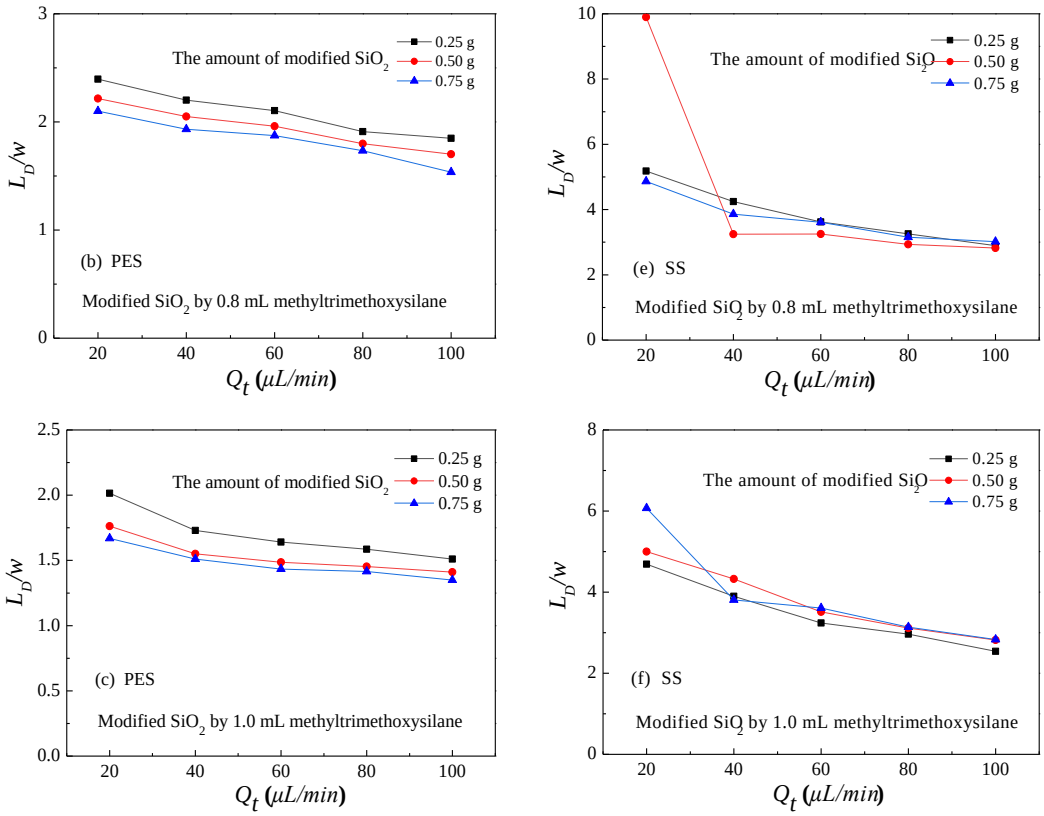

Fig. 12. Effects of the flow rate on length of dispersed phase droplets in PES (a-c) and SS (d-f) at a flow rate ratio of 1:1

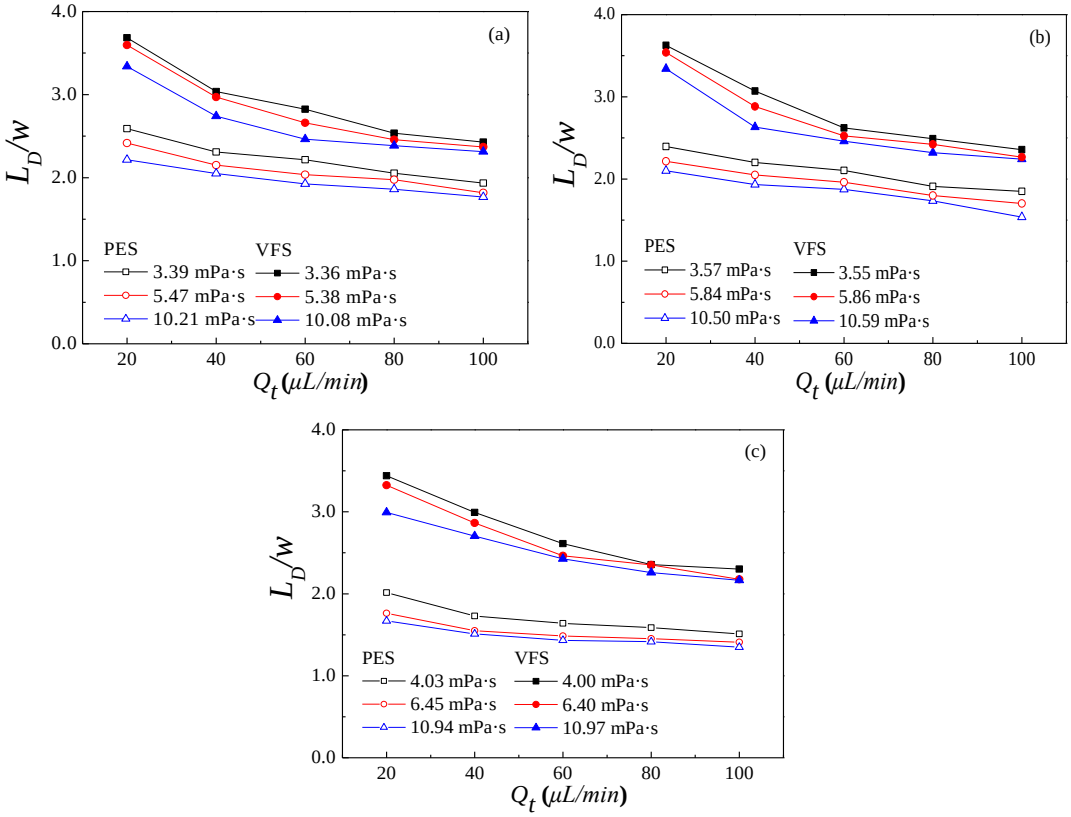

Fig. 13. Comparison of L_D/w of VFS and PES at a flow rate ratio of 1:1

3.6 Empirical correlation for the length of the dispersed droplet

It was interesting that the size of the dispersed W/S/O spherical emulsion droplets ($Ph_{2\text{-}1}$) played an important role on the formation of the dispersed Pickering emulsion phase (Ph_2). The possible reason was that the complicating movement of $Ph_{2\text{-}1}$ in Ph_2, the interaction between adjacent $Ph_{2\text{-}1}$, and the rigid shell of $Ph_{2\text{-}1}$ under the balance of all forces in the above discussion. Compared with conventional homogeneous dispersed phase, the dynamic behaviors of the dispersed Pickering emulsion made of $Ph_{2\text{-}1}$ and the continuous ethyl acetate phase ($Ph_{2\text{-}2}$) were more complex. Although many rational models based on classical Garstecki's scale law model have been proposed in the previous literatures for the squeezing regime (Garstecki et al., 2006; van Steijn et al., 2007; Leclerc et al., 2010; Xiong et al., 2007; Shao et al., 2008), the shearing regime (de Menech et al., 2008; Guo and Chen, 2009; Thorsen et al., 2001; Husny and Cooper-White, 2006; Xu et al., 2008) and the transition squeezing/shearing regime (Christopher et al., 2008; de Menech et al., 2008; Xu et al., 2008; Fu et al., 2010), these models were difficult to extrapolate to those complex systems involving internal movement in the dispersed phase-Pickering emulsion.

Considering the complexity of the movement of $Ph_{2\text{-}1}$ in Ph_2, moreover, our investigation for the application of Pickering emulsion in microchannels was only in the preliminary stage, so the rational model for predicting the length of the dispersed droplet (L_D/w) was difficult to be proposed. Based on the rule of thumb, the empirical correlation would be adopted in this work. Essentially, our proposed empirical

correlation still originated from classical Garstecki's scale law model. Meanwhile, several classical and latest models were introduced to compare with our empirical model and the experimental results, as shown in Fig. 15. It was obvious that the predicted values from previous models were rather larger than the experimental results. The main reason for the difference was the negative effects of $Ph_{2\text{-}1}$ on the break-up of the dispersed phase at the T-junction, that is, the existence of $Ph_{2\text{-}1}$ in Ph_2 impeded the formation of Ph_2. So, the viscosity ratio and *Ca* were adopted in the empirical correlation.

These slug droplets were formed under squeezing ($Ca<1.5\times10^{-3}$). The experimental results showed that the length of the dispersed droplet was affected by the viscosity ratio and *Ca*, and the change of the viscosity of Ph_2 affected the size and movement of $Ph_{2\text{-}1}$ in Ph_2. That is, the intrinsic mechanism of the above influence of fluid viscosity on droplet formation could be attributed to the external shear stress and the movement behavior of $Ph_{2\text{-}1}$ in Ph_2. So these two important dimensionless numbers were introduced on the basis of the prediction formula mentioned in the literature, the results showed that droplet size of all systems could be predicted well.

In order to establish a scaling law for the Pickering emulsion flow, an empirical correlation was developed for the flow characteristic number L_D/w with a wider range of fluidic parameters, by introducing two additional dimensionless numbers, $Ca=\mu_c u_c/\gamma$, and $\lambda=\mu_d/\mu_c$, based on the experimental investigations. Fig. 14 shows experimental results for L_D/w as a function of *Ca* at three levels of viscosity ratio (λ) with a given flow rate of the dispersed phase (Q_d) and hydrophobicity of SiO_2 particle

surface. The experimental results for a wider range of operating conditions are presented in SI (Figs. S6-S7).

As shown in Fig. 14(a), initially, L_D/w dropped sharply with the increase of Ca, followed by gradually leveling off as $Ca>1.5\times10^{-3}$. With given Q_d (20 μL/min) and λ, the increase in Ca reflected a higher flow rate of the continuous phase (Q_c), speeding up the contraction of the phase interface while reducing the detachment time of the droplet, finally leading to the decrease of L_D/w. For given Ca and Q_d, the decrease of λ resulted in increase of L_D/w, where the lower viscosity of the dispersed phase was in favor of the pinch-off of the neck while taking a shorter period of time to complete the formation of the dispersed droplet.

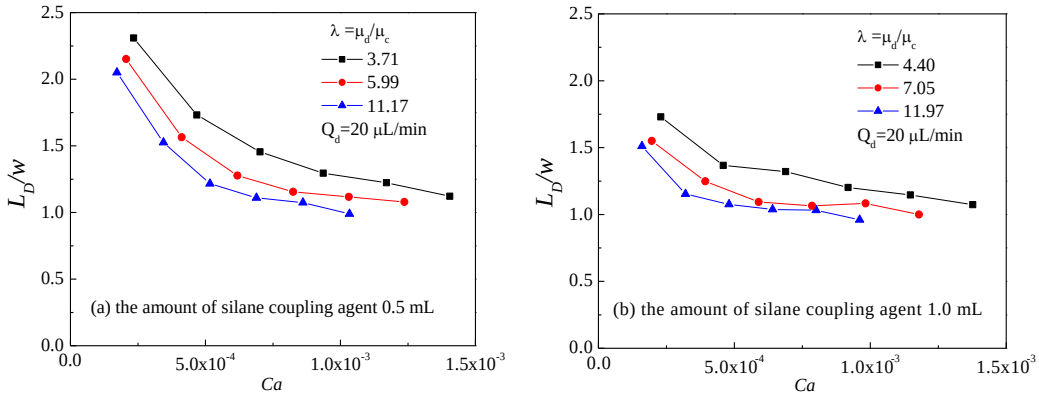

Fig. 14. L_D/w vs. Ca at different λ and SO_2 particle hydrophobicity levels with a given Q_d for PES

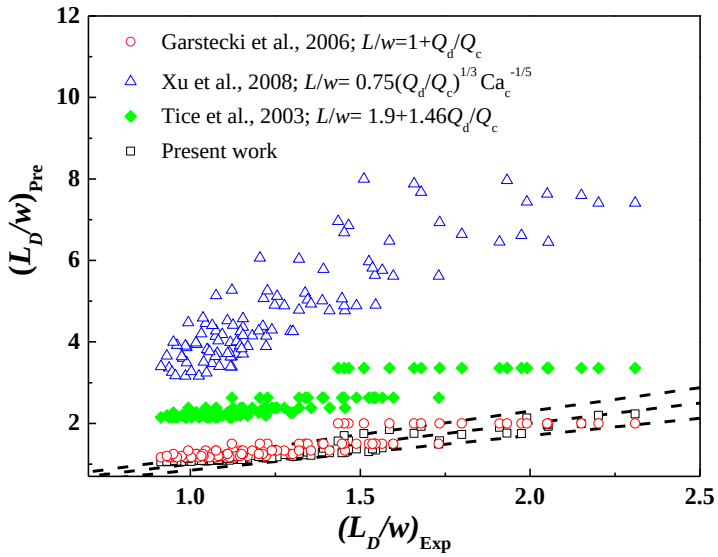

Fig. 15. Comparison of L_D/w between the fitting results from Eq. (1) and the references, $1.6\times10^{-4}<Ca<3.0\times10^{-3}$

As demonstrated above, the droplet length in terms of L_D/w was significantly influenced by viscosity and volumetric flow rates of the two phases, liquid properties and interfacial tension within a confined microchannel. Based on the experimental measurements, a scaling law was proposed for L_D/w by considering those key parameters. By using a multi-variable least squares method to fit all the experimental data, an empirical correlation was obtained (Eq. (1)). For comparison, an empirical correlation for VFS was also carried out (Eq. (2)). It was also interesting that the value of the exponents might be indicative of the influence of the leakage flow at the corner of microchannel, which may also be associated with the defects of the empirical correlation.

$$\text{PES:}\quad \frac{L_D}{w}=1+0.08\left(\frac{\mu_d}{\mu_c}\right)^{-0.56}\left(\frac{Q_d}{Q_c}\right)^{0.91}Ca^{-0.41} \tag{1}$$

$$\text{VFS:}\quad \frac{L_D}{w}=1+0.17\left(\frac{\mu_d}{\mu_c}\right)^{-0.36}\left(\frac{Q_d}{Q_c}\right)^{0.45}Ca^{-0.40} \tag{2}$$

The empirical correlations show that L_D/w is more dependent on Q_d/Q_c than Ca and λ for both PES and VFS. Compared to VFS, the effects of Q_d/Q_c and λ on L_D/w are larger for PES than VFS. Interestingly, Ca plays an almost equivalent role in influencing L_D/w for PES and VFS. The reason behind this phenomenon is worth investigating further.

The validation of the two correlation models, Eq. (1) & (2), was conducted by comparing the predicted values and experimental results of L_D/w (Fig. 16). It can be seen that the relative errors of the predictions for L_D/w all fall within ±15% for both PES and VFS. Considering the uncertainty associated with experimental quantification of L_D/w, the predicted values were in satisfactory agreement with the experimental data. These results indicated that the scaling law could be applied to predict L_D/w for droplet/slug flow in microfluidic T-junction with an acceptable accuracy.

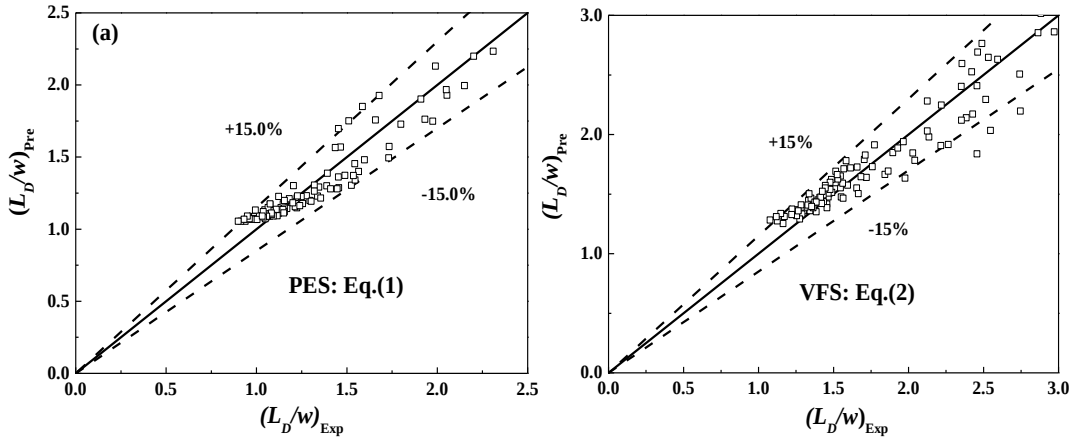

Fig. 16. Comparison of the predicted values and the experimental data for PES and VFS

4. Conclusion

The clogging and difficulties in achieving stable operation in multiphase flow involving solid micro/nano particles are still severe challenges for heterogeneous

catalytic reactions or other multiphase processes in microchannel reactors. To address those challenges, the Pickering emulsion was adopted in the present work. The microfluidic behavior and hydrodynamics of Pickering emulsion systems (PES) within a microchannel reactor were systematically characterized, both experimentally and theoretically, under a range of operating conditions. For comparison, a suspension system (SS) formed with ethyl acetate containing suspended SiO_2 nanoparticles and water, and a viscous fluid system (VFS) consisting of ethyl acetate, methyl-silicone oil and water, were also examined.

(1) Liquid-liquid two-phase flow hydrodynamics of PES, SS and VFS around the T-junction within the main microchannel were dependent on a range of parameters, including surface hydrophobicity of stabilizing SiO_2 nanoparticles, amount of SiO_2 particles added, viscosity and flow rate.

(2) Four flow patterns of parallel flow Slug flow, monodispersed droplet flow, and jetting droplet flow were observed under these operating conditions for PES and VFS, where superficial velocity was the key factor affecting the flow patterns transition. The dispersed droplets were prone to adhere to the channel wall for SS, which made the interface be elongated and deformed, even block the channel.

(3) The formation of slug flow was the result of the dynamic competition among the inertia force (F_c, F_d), the interfacial force (F_γ), the viscous shearing force (F_μ) and the continuous phase pressure (P_{neck}, P_{tip}).

(4) The motion behavior of interface $Ph_{2\text{-}1}$ was determined by drag force (F_D), interfacial tension at the S/O interface (σ), confinement of the microchannel wall,

Basset force (F_{Ba}), virtual mass force (F_{VM}), Magnus force (F_M), Saffman force (F_{Sa}), and collision and the repulsion forces between the adjacent emulsion droplets. The motion trajectory showed the characteristics of the approximate clockwise direction and the straight line.

(5) A scaling law of the droplet size (L_D/w) was developed as a function of Q_d/Q_c, μ_d/μ_c and Ca. The results showed that the predicted values were in accordance with the experimental data.

SUPPORTING INFORMATION

Experimental data under other operating conditions are shown in Supporting Information.

Acknowledgements

We gratefully acknowledge the financial supports from National Natural Science Foundation of China (Nos. 21978250, 21808194), Natural Science Foundation of Shandong Province (ZR2017BB058) and Key Technology Research and Development Program of Shandong (2019JZZY010410).

Nomenclature

$A_{Ph2\text{-}1}$	Cross-sectional area of $Ph_{2\text{-}1}$, m^2
Ca	Capillary number, $Ca=\mu_c u_c/\gamma$
C_D	Drag coefficient
d	Pickering emulsion droplet diameter, μm
d_H	Hydraulic diameter, m
F_{Ba}	Basset force, N
F_c	Inertia force caused by Ph_1, N
F_d	Inertia force caused by Ph_2, N
F_D	Drag force, N

F_M	Magnus force, N
F_{Sa}	Saffman force, N
F_{VM}	Virtual mass force, N
$F_{\gamma,\ neck}$	Interfacial force on the neck, N
F_μ	Viscous shearing force, N
j_c	Superficial velocity of the continuous phase, mm/s
j_d	Superficial velocity of the dispersed phase, mm/s
L_D	Length of the dispersed phase droplets, μm
M	Amount of methyltrimethoxysilane, mL
Ph_1	Continuous water phase
Ph_2	Dispersed Pickering emulsion phase
$Ph_{2\text{-}1}$	Dispersed W/S/O spherical emulsion droplets
$Ph_{2\text{-}2}$	Continuous ethyl acetate phase
P_{neck}	Continuous phase pressure on the neck of Ph_2, N/m^2
P_{tip}	Continuous phase pressure on the tip of Ph_2, N/m^2
Q_c	Flow rate of the continuous phase, μL/min
Q_d	Flow rate of the dispersed phase, μL/min
Q_t	Total flow rate of two phases, μL/min
$@S$	Amount of modified SiO_2, g
t	Time, ms
u	Superficial velocity, m/s
w	Microchannel width, μm
Greek letters	
γ	Interfacial tension, mN/m
δ_{neck}	Thickness of the emerging Ph_2 tip, m
δ_{gap}	Gap between the wall and the dispersed phase, m
μ	Dynamic viscosity, mPa·s
λ	Two-phase viscosity ratio, $\lambda=\mu_d/\mu_c$
ρ	Density, kg/m^3
σ	Interfacial tension at the S/O interface, mN/m

References

Abadie, T., Xuereb, C., Legendre, D., Aubin, J., 2013. Mixing and recirculation characteristics of gas-liquid Taylor flow in microreactors. Chem. Eng. Res. Des. 91, 2225-2234.

Adamo, A., Beingessner, R.L., Behnam, M., Chen, J., Jamison, T.F., Jensen, K.F., Monbaliu, J.C.M., Myerson, A.S., Revalor, E.M., Snead, D.R., Stelzer, T., Weeranoppanant, N., Wong, S.Y., Zhang, P., 2016. On-demand continuous-flow production of pharmaceuticals in a compact, reconfigurable system. Science 352, 61-67.

Archibong-Eso, A., Shi, J., Baba Y.D., Aliyu, A.M., Raji, Y.O., Yeung, H., 2019. High viscous oil-water two-phase flow: experiments and numerical simulations. Heat Mass Transfer 55, 755-767.

Aveyard, R., Binks, B.P., Clint, J.H., 2003. Emulsions stabilised solely by colloidal

particles. Adv. Colloid. Interface 100, 503-546.
Bai, L., Fu,Y.H., Zhao S.F., Cheng Y., 2016. Droplet formation in a microfluidic T-junction involving highly viscous fluid systems. Chem. Eng. Sci. 145, 141-148.
Binks, B.P., Lumsdon, S.O., 2000. Influence of particle wettability on the type and stability of surfactant-free emulsions. Langmuir 16, 8622-8631.
Binks, B.P., Lumsdon, S.O., 2001. Pickering emulsions stabilized by monodisperse latex particles: effects of particle size. Langmuir 17, 4540-4547.
Binks, B.P., Whitby, C.P., 2004. Silica particle-stabilised emulsions of silicone oil and water: aspects of emulsification. Langmuir. 20, 1130-1137.
Binks, B.P., Whitby, C.P., 2005. Nanoparticle silica-stabilised oil-in-water emulsions: improving emulsion stability. Colloid. Surface. A., 253, 105-115.
Binks, B.P., Fletcher, P.D.I., Holt, B.L., Kuc, O., Beaussoubre, P., Wong, K., 2010. Compositional ripening of particle-and surfactant-stabilised emulsions: a comparison. Phys. Chem. Chem. Phys. 12, 2219-2226.
Cao Z., Wu Z., Sundén, B., 2018. Dimensionless analysis on liquid-liquid flow patterns and scaling law on slug hydrodynamics in cross-junction microchannels. Chem. Eng. J. 344 604-615.
Chang, F.Q., Vis, C.M., Ciptonugroho, W., Bruijnincx, P.C.A., 2021. Recent developments in catalysis with Pickering Emulsions. Green Chem., DOI: 10.1039/D0GC03604H.
Christopher, G.F., Noharuddin, N.,N., Taylor, J.A., Anna, S.L., 2008. Experimental observations of the squeezing-to-dripping transition in T-shaped microfluidic junctions. Phy. Rev. E 78, 036317.
Crossley, S., Faria, J., Shen, M., Resasco, D.E., 2010. Solid nanoparticles that catalyze biofuel upgrade reactions at the water/oil interface. Science. 327, 68-72.
Cubaud, T., Mason, T.G., 2008. Capillary threads and viscous droplets in square microchannels. Phys. Fluids 20, 053302.
de Menech, M., Garstecki, P., Jousse, F., Stone, H.A., 2008. Transition from squeezing to dripping in a microfluidic T-shaped junction. J. Fluid Mech., 595, 141-161.
Fu, T.T., Ma, Y.G., Funfschilling, D., Zhu, C.Y., Li, H.Z., 2010. Squeezing-to-dripping transition for bubble formation in a microfluidic T-junction. Chem. Eng. Sci. 65, 3739-3748.
Fu T.T., Wei L.J., Zhu C.Y., Ma Y.G., 2015. Flow patterns of liquid-liquid two-phase flow in non-Newtonian fluids in rectangular microchannels. Chem. Eng. Process. 91, 114-120.
Garstecki, P., Fuerstman, M.J., Stone, H.A., Whitesides, G.M., 2006. Formation of droplets and bubbles in a microfluidic T-junction—scaling and mechanism of break-up. Lab Chip, 6, 437-446.
Guo, F., Chen, B., 2009. Numerical study on Taylor bubble formation in a micro-channel T-junction using VOF method. Microgravity Sci. Technol. 21, S51-S58.
Husny, J., Cooper-White, J.J., 2006. The effect of elasticity on drop creation in T-shaped microchannels. J. Non-Newtonian Fluid Mech. 137, 121-136.
Jähnisch, K., Hessel, V., Löwe, H., Baerns, M., 2004. Chemistry in microstructured reactors. Angew. Chem. Int. Ed. 43, 406-446.
Jin, N., Yue J., Zhao, Y.C., Lv, H.Y., Wang, C.X., 2020. Experimental study and mass transfer modelling for extractive desulfurization of diesel with ionic liquid in microreactors. Chem. Eng. J. doi.org/10.1016/j.cej.2020.127419.
Kececi, S., Wörner, M., Onea, A., Soyhan H.S., 2009. Recirculation time and liquid

slug mass transfer in co-current upward and downward Taylor flow. Catal. Today 147, S125-S131.
Kim, Y.W., Yoo, J.Y., 2012. Transport of solid particles in microfluidic channels. Opt. Lasers Eng. 50, 87-98.
Kobayashi, J., Mori, Y., Okamoto, K., Akiyama, R., Ueno, M., Kitamori, T., Kobayashi, S., 2004. A microfluidic device for conducting gas-liquid-solid hydrogenation reactions. Science 304, 1305-1308.
Leclerc, A., Philippe, R., Houzelot, V., Schweich, D., de Bellefon, C., 2010. Gas-liquid Taylor flow in square micro-channels: New inlet geometries and interfacial area tuning. Chem. Eng. J. 165, 290-300.
Leclercq, L., Mouret, A., Proust, A., Schmitt, V., Bauduin, P., Aubry, J.M., Nardello-Rataj, V., 2012. Pickering emulsion stabilized by catalytic polyoxometalate nanoparticles: A new effective medium for oxidation reactions. Chem. Eur. J. 18, 14352-14358.
Liedtke, A.K., Bornette, F., Philippe, R., Bellefon, C.D., 2013. Gas-liquid-solid "slurry Taylor" flow: Experimental evaluation through the catalytic hydrogenation of 3-methyl-1-pentyn-3-ol. Chem. Eng. J. 227, 174-181.
Liedtke, A.K., Scheiff, F., Bornette, F., Philippe, R.G., Agar, D.W., Bellefon, C.D., 2015. Liquid-solid mass transfer for microchannel suspension catalysis in gas-liquid and liquid-liquid segmented flow. Ind. Eng. Chem. Res. 54, 4699-4708.
Liu, H., Wang, C.Y., Zou, S.W., Wei, Z.J., Tong, Z., 2012. Facile fabrication of polystyrene/halloysite nanotube microspheres with core-shell structure via Pickering suspension polymerization. Polymer Bulletin 69, 765-777.
Liu, W., Zhao, Y.J., Zeng, C.F., Wang, C.Q., Serra, C.A., Zhang, L.X.,2017. Microfluidic preparation of yolk/shell ZIF-8/alginate hybrid microcapsules from Pickering emulsion. Chem. Eng. J. 307, 408-417.
Márquez, N., Moulijn, J., Makkee, M., Kreutzer, M.T., Castaño, P., 2019. Tailoring the multiphase flow pattern of gas and liquid through micro-packed bed of pillars. React. Chem. Eng. 4, 838-851.
Meng, Y., Sun, W.X., Yang, H., Wang, W., Jin, N., Zhang, X.L., Zhao, Y.C., Lv, H.Y., 2020. Fine tuning of surface properties of SiO_2 nanoparticles for the regulation of Pickering emulsions. Colloid. Surface. A. 592, 124603.
Munirathinam, R., Huskens, J., Verboom, W., 2015. Supported catalysis in continuous-flow microreactors. Adv. Synth. Catal. 357, 1093-1123.
Pan, D.W., Liu, M.F., Li, F., Chen, Q., Liu, X.D., Liu, Y.Y., Zhang, Z.W., Huang, W.X., Li, B., 2018. Formation mechanisms of solid in water in oil compound droplets in a horizontal T-junction device. Chem. Eng. Sci. 176, 254-263.
Qi, L., Luo, Z., Lu, X., Facile synthesis of starch-based nanoparticle stabilized Pickering emulsion: its pH-responsive behavior and application for recyclable catalysis. Green Chem. 2018, 20:1538-50.
Shao, N., Salman, W., Gavriilidis, A., Angeli, P., 2008. CFD simulations of the effect of inlet conditions on Taylor flow formation. Int. J. Heat Fluid Flow 29, 1603-1611.
Shen, M., Resasco, D.E., 2009. Emulsions stabilized by carbon nanotube-silica nanohybrids. Langmuir 25, 10843-10851.
Su, Y.H., Chen, G.W., Yuan, Q., 2012. Influence of hydrodynamics on liquid mixing during Taylor flow in a microchannel. AIChE J. 58, 1660-1670.
Tanimu, A., Jaenicke, S., Alhooshani, K., 2017. Heterogeneous catalysis in continuous flow microreactors: A review of methods and applications. Chem. Eng. J. 327,

792-821.
Thorsen, T., Roberts, R.W., Arnold, F.H., Quake, S.R., 2001. Dynamic pattern formation in a vesicle-generating microfluidic device. Phy. Rev. Lett. 86, 4163-4166.
Tice, J.D., Song, H., Lyon, A.D., Ismagilov, R.F., 2003. Formation of droplets and mixing in multiphase microfluidics at low values of the Reynolds and the capillary numbers. Langmuir 19, 9127-9133.
Tidona, B., Desportes, S., Altheimer, M., Ninck, K., von Rohr, P.R., 2012. Liquid-to-particle mass transfer in a micro packed bed reactor. Int. J. Heat Mass Transfer 55, 522-530.
Tsaoulidis, D., Dore, V., Angeli, P., Plechkova, N.V., Seddon, K.R., 2013. Flow patterns and pressure drop of ionic liquid-water two-phase flows in microchannels. Int. J. Multiphase Flow 54, 1-10.
Vadivukkarasan, M., Dhivyaraja, K., Panchagnula, M.V., 2020. Breakup morphology of expelled respiratory liquid: From the perspective of hydrodynamic instabilities. Phys. Fluids 32, 094101.
van Steijn, V., Kreutzer, M.T., Kleijn, C.R., 2007. μ-PIV study of the formation of segmented flow in microfluidic T-junctions. Chem. Eng. Sci. 62, 7505-7514.
Vis, C.M., Nieuwelink, A.E., Weckhuysen, B.M., Bruijnincx, P.C.A., 2020. Continuous flow Pickering emulsion catalysis in droplet microfluidics studied with in situ Raman microscopy. Chem. Eur. J. 26, 15099-15102.
Wang, H. Shen, Q.y., Zhu, C.Y., Ma, Y.G., Fu. T.T., 2021. Formation and uniformity of bubbles in highly viscous fluids in symmetric parallel microchannels. Chem. Eng. Sci. 230, 116166.
Wu, J., Ma G.H., 2016. Recent studies of Pickering emulsions: particles make the difference. Small 12, 4633-4648.
Wang, K., Lv, Y.C., Yang, L., Luo, G.S., 2013. Microdroplet coalescences at microchannel junctions with different collision angles. AIChE J. 59, 643-649.
Wang, Z.P., van Oers, M.C.M., Rutjes, F.P.J.T., van Hest, J.C.M., 2012. Polymersome colloidosomes for enzyme catalysis in a biphasic system. Angew. Chem. Int. Ed. 124, 10904-10908.
Xiao, F., Dianat, M., McGuirk, J.J., 2016. A robust interface method for drop formation and breakup simulation at high density ratio using an extrapolated liquid velocity. Comput. Fluids 136, 402-420.
Xiong, R.Q., Bai, M., Chung, J.N., 2007. Formation of bubbles in a simple co-flowing micro-channel. J. Micromech. Microeng. 17, 1002-1011.
Xu, J.H., Li, S.W., Tan, J., Luo, G.S., 2008. Correlations of droplet formation in T-junction microfluidic devices: from squeezing to dripping. Microfluid. Nanofluid. 5, 711-717.
Yagodnitsyna, A.A., Kovalev, V.A., Bilsky, V.A., 2016. Flow patterns of immiscible liquid-liquid flow in a rectangular microchannel with T-junction. Chem. Eng. J. 303, 547-554.
Yang, H.Q., Fu, L.M., Wei, L.J., Liang, J.F., Binks, B.P., 2015. Compartmentalization of incompatible reagents within Pickering emulsion droplets for one-pot cascade reactions. J. Am. Chem. Soc. 137, 1362-1371.
Yang, X.M., Wang, X.N., Qiu, J.S., 2010. Aerobic oxidation of alcohols over carbon nanotube-supported Ru catalysts assembled at the interfaces of emulsion droplets. Appl. Catal. A-Gen. 382, 131-137.
Yao, C.Q., Zhao, Y.C., Chen, G.W., 2018. Multiphase processes with ionic liquids in microreactors: hydrodynamics, mass transfer and applications. Chem. Eng. Sci.

189, 340-359.
Yue, J., 2017. Multiphase flow processing in microreactors combined with heterogeneous catalysis for efficient and sustainable chemical synthesis. Catal. Today 308, 3-19.
Zaloha, P., Kristal, J., Jiricny, V., Völkel, N., Xuereb, C., Aubin, J., 2012. Characteristics of liquid slugs in gas-liquid Taylor flow in microchannels. Chem. Eng. Sci. 68, 640-649.
Zhang, M., Wei, L., Chen, H., Du, Z., Binks, B. P., Yang, H., 2016. Compartmentalized droplets for continuous flow liquid-liquid interface catalysis. J. Am. Chem. Soc. 138, 10173-10183.
Zhang, Q., Liu, H.C., Zhao, S.N., Yao, C.Q., Chen, G.W., 2019. Hydrodynamics and mass transfer characteristics of liquid-liquid slug flow in microchannels: The effects of temperature, fluid properties and channel size. Chem. Eng. J. 358, 794-805.
Zhang, Q.D., Zhu, C.Y., Du, W., Liu, C., Fu, T.T., Ma, Y.G., Li, H.Z., 2018. Formation dynamics of elastic droplets in a microfluidic T-junction. Chem. Eng. Res. Des. 139, 188-196.
Zhao, Y.C., Chen, G.W., Yuan, Q., 2006. Liquid-liquid two-phase flow patterns in a rectangular microchannel. AIChE J. 52, 4052-4060.
Zhao, Y.C., Chen, G.W., Ye, C.B., Yuan, Q., 2013. Gas-liquid two-phase flow in microchannel at elevated pressure. Chem. Eng. Sci. 87, 122-132.

Hydrodynamic characterization of continuous flow of Pickering droplets with solid nanoparticles in microchannel reactors

Wenxing Sun[a], Xunli Zhang[b], Chaoqun Yao[c], Qingqiang Wang[a], Nan Jin[a], Hongying Lv[a], Yuchao Zhao[a,*]

[a] Shandong Engineering Research Center of Green Manufacturing for New Chemical Materials, College of Chemistry & Chemical Engineering, Yantai University, Yantai 264005, China

[b] School of Engineering & Institute for Life Sciences, University of Southampton, Southampton SO17 1BJ, UK

[c] Dalian National Laboratory for Clean Energy, Dalian Institute of Chemical Physics, Chinese Academy of Sciences, Dalian 116023, China

Abstract

In this work, a method based on Pickering emulsion systems (PES) was proposed to manipulate multiphase processes containing solid particles in microchannels without adhesion and/or accumulation. The flow hydrodynamics of PES in a microchannel were systematically characterized. For comparison, a suspension system (SS, ethyl acetate with suspended SiO_2 nanoparticles-water) and a viscous fluid system (VFS, ethyl acetate with methyl-silicone oil-water) were examined. It was found liquid-liquid two-phase characteristics of PES, SS and VFS around T-junction within the main microchannel depended on surface hydrophobicity of stabilizing SiO_2 nanoparticles, amount of SiO_2 particles added, viscosity and flow rate. Four flow patterns were observed under these operating conditions for PES and VFS, where superficial velocity was the key factor affecting the flow patterns transition. Finally, a scaling law of the droplet size was established as a function of Q_d/Q_c, μ_d/μ_c and Ca.

Keywords: Microchannel reactors, Hydrodynamics, Pickering emulsion, Solid

* Corresponding Author. Tel: +86 535 6903386.
E-mail address: yczhao@ytu.edu.cn (Y. Zhao).

particles, Slug flow

1. Introduction

With the development of microchannel reactor technology for chemical process intensification and optimization, multiphase flow hydrodynamics, transport and reaction characteristics under microfluidic condition have received much attention and been intensively investigated over the past two decades (Jähnisch et al., 2004; Chen et al., 2006; Wang et al., 2013; Adamo et al., 2016; Jin et al., 2020). Compared with conventional macroscale reactors, the microreactor has demonstrated many advantages such as large specific interfacial area, fast heat and mass transfer rate, improved safety and controllability, and reduced backmixing. At present, the vast majority of work on multiphase systems in microreactors has been focused on gas-liquid and liquid-liquid processes, but limited work has been performed on continuous microfluidics for transporting solid particles across microchannel networks (Xu et al., 2008; Kim and Yoo, 2012; Zaloha et al., 2012; Abadie et al., 2013; Liedtke et al., 2013; Zhao et al., 2013; Yao et al., 2018). This is largely associated with (i) the characteristic microchannel geometry, (ii) the large surface area/volume ratio of microchannels, and (iii) the large surface energy of solid micro/nano particles. Consequently, those factors can result in clogging of microchannels by mechanical obstruction and/or adhesion of solid particles to microchannel surfaces, leading to unstable or uncontrollable flow and mass transfer processes. In view of the significance of heterogeneous chemical processes in the chemical industry, especially heterogeneous catalytic reactions involving solid catalyst particles, there is a

tremendous need to address the above challenges in order to effectively facilitate heterogeneous catalysis in microchannel reactors (Munirathinam et al., 2015; Tanimu et al., 2017; Yue., 2017).

To investigate microfluidic multiphase processes involving gas-liquid flow through microchannels filled with solid catalyst particles, Márquez et al. (2019) designed a series of micro-packed beds of solid particles and pillars. The gas-liquid two-phase flow hydrodynamics and the corresponding mass transfer rate were characterized by varying gas/liquid flow rates and the distance between pillars, together with the liquid hold-up and gas-liquid interfacial area. In another micro-packed bed reactor, Tidona et al. (2012) elucidated the liquid-to-particle mass transfer characteristics with a copper dissolution method by adjusting the ratio of hydraulic to particle diameter and the channel geometries. They demonstrated the enhancement of the gas-liquid-solid three-phase mass transfer performance and the heterogeneous reaction rate, which were attributed to the existence of the fixed catalyst particles. Along with those developments, however, there still remain some technical issues for the practical application of such micro-packed bed reactors, in terms of difficult replacement of the solid catalyst, poor controllability of multiphase flow, and large pressure drop.

Accordingly, a micro-suspended reactor configuration has been proposed. Liedtke et al.(2013, 2015) developed a micro-suspended reactor where solid catalyst particles were suspended in the fluid under Taylor flow, for the catalytic hydrogenation of methyl pentanol. However, the suspended solid particles were found to cause some significant problems including poor flow stability, frequent clogging of channels

when the solid catalyst suspension started to aggregate, and deposition of solid particles to the channel wall surface. Further, Kobayashi et al. (2004) developed a wall-coated microreactor with a very thin layer of catalyst particles coated onto the inner wall of microchannel, for conducting gas-liquid-solid hydrogenation reactions achieving a high conversion. Although the wall-coated microreactor had advantages in eliminating clogging and also reducing pressure drop, it suffered from some inherent drawbacks, such as low catalyst loading per unit volume, catalyst loss, and difficulties in refreshing or replacing the deactivated catalyst.

In recent years, the introduction of the Pickering emulsion into microchannel reactors has opened up new avenues for manipulating and controlling multiphase flow systems, in particular, to address the above mentioned challenges associated with involvement of solid particles in microchannel reactors (Liu et al., 2017; Vis et al., 2020). Differing from the traditional emulsion, the Pickering emulsion is stabilized by micro/nano solid particles (instead of liquid surfactants) with selected hydrophilicity or hydrophobicity, that help eliminate operating difficulties associated with traditional surfactants, such as the formation of foaming, difficulty in emulsifier separation, and product contamination. The Pickering emulsion has also a unique interface self-assembly property for micro/nano particles, reducing the possibility of collision and coalescence between the adjacent emulsion droplets (Leclercq et al., 2012; Yang et al., 2015). Furthermore, it is a thermodynamically stable system (Aveyard et al., 2003) with insignificant influence by the environmental conditions such as temperature and salt ion concentration. Most importantly, the surface energy of

micro/nano particles is released at the interface of liquid-solid, reducing the possibility of their adherence to the channel wall and their aggregation towards consequent clogging. When these micro/nano particles are functionalized as solid catalysts, droplet-based heterogeneous catalytic systems are formed having large liquid-solid two-phase interface and significantly reduced internal diffusion resistance (Shen et al., 2009; Crossley et al., 2010; Yang et al., 2010; Wang et al., 2012). Thus, the Pickering emulsion systems have been applied to oxidation, hydrogenation, condensation and enzyme catalysis for gas-liquid or liquid-liquid two-phase systems, due to their ultra-stable and large interface, biological compatibility and environmental friendliness (Zhang et al., 2016; Qi et al., 2018; Chang et al., 2021). Factually, the application of Pickering emulsion in heterogeneous catalytic reaction is still in the preliminary stage, and its prospects are worthy of being further investigated and explored. Recently, Vis et al. (2020) reported the first use of a tube-in-tube co-flow microfluidic approach for flow Pickering emulsion catalysis, which showed a nine-fold improvement in yield compared to the simple biphasic flow system offering a versatile new extension of Pickering emulsion catalysis. Nevertheless, to realize the full potential of the Pickering emulsion for applications in microchannel reactors it is essential to gain a fundamental understanding of the multiphase flow characterization involving solid particles within microreactors, which is lacking at present, however.

Built on our previous research on a Pickering emulsion-water system (PES) stabilized by SiO_2 nanopartricles with tunable surface properties (Meng et al., 2020), the present study aimed to systematically characterize the microfluidic behavior and

hydrodynamics of Pickering emulsions within microreactors under a range of operating conditions. For comparing with the PES, a suspension system (SS) formed with ethyl acetate containing suspended SiO_2 nanoparticles and water, and a viscous fluid system (VFS) consisting of ethyl acetate, methyl-silicone oil and water, were employed. A qualitative force analysis was carried out to gain insight into the mechanism of the flow pattern transition and the motion behavior of emulsion droplets. Furthermore, a dimensionless characteristic number L_D/w (i.e., length of dispersed phase droplet/width of microchannel) was investigated in order to establish a scaling law through empirical correlation.

2. Experimental section

SiO_2 nanoparticles (20 nm, Beijing Shenghe Haoyuan Technology Co., Ltd), methyltrimethoxysilane (Aladdin, CAS 1185-55-3) and ethyl acetate-water system (Sinopharm Chemical Reagent Co., Ltd, CAS 141-78-6) were chosen to prepare the stable Pickering emulsion according to our previous studies (Meng et al., 2020). In a typical process of surface modification of SiO_2 particles, raw SiO_2 particles (1.0 g), methyltrimethoxysilane (with selected amount) and toluene (30 mL) were successively added into the reactor vessels (100 mL) made of stainless steel. The six vessels in the unit contained either the same mixture for increasing production, or different ones for examining multiple parameters. The rotating unit, placed in a forced convection oven (KLJX-8a, Yantai Branch Chemical Equipment Co., Ltd) set at 130 ^oC, operated at an optimized rotating rate of 10 Hz for 12 h. The silanol group on the surface of SiO_2 particles underwent condensation reaction with the silane coupling

agent, with the increase of the amount of silane coupling agent, more hydrophobic groups were grafted on the surface of particles, so that the hydrophobicity became stronger. The surface of SiO_2 nanoparticles were modified to reduce its hydrophilicity by the surface grafting method with different amounts of methyltrimethoxysilane, i.e. 0.5 mL, 0.8 mL and 1.0 mL, denoted as M0.5, M0.8 and M1.0, respectively. During the preparation of the emulsion, the oil-water volumetric ratio of ethyl acetate to water was fixed at 7:5 and the amount of modified SiO_2 particles (0.25 g, 0.5 g and 0.75 g) was adjusted to prepare the W/O (water/oil) Pickering emulsions with different viscosity. Pickering emulsion exhibited great stability, it was found that droplets deposited at the oil phase bottom, but the droplet size did not change significantly after standing for 24 hours. The emulsions samples prepared were denoted as M0.5@S0.25, M0.5@S0.5, M0.5@S0.75, M0.8@S0.25, M0.8@S0.5, M0.8@S0.75, M1.0@S0.25, M1.0@S0.5, M1.0@S0.75, as shown in Table 1.

The contact angle of the Pickering emulsion was measured by an optical tensiometer (JC2000, Shanghai Zhongchen Digital Technology Equipment Co., Ltd) to quantify the hydrophobicity or hydrophilicity of the modified particle surface. The viscosity of Pickering emulsion was measured by a rotational viscometer (Brookfield DV2T, USA) at 24 ^{o}C. The interfacial tension between the continuous phase (water) and the dispersed phase (the Pickering emulsion) was measured by an interfacial tensiometer (DataPhysics OCA 15EC, Germany). The uncertainty of measurement was less than ±5%. Table 1 summarizes these measured physical properties of the three multiphase systems, namely, PES, SS and VFS, in terms of viscosity, interfacial

tension and droplet diameter.

Table 1. Physical properties of PES, SS and VFS

Testing system (24 ºC)		Viscosity μ(mPa·s)	Interfacial tension γ (mN/m)	Droplet diameter d (μm)
PES	M0.5@S0.25	3.39	7.64	171.88
	M0.5@S0.5	5.47	7.15	55.21
	M0.5@S0.75	10.21	7.00	41.67
	M0.8@S0.25	3.57	7.24	122.19
	M0.8@S0.5	5.84	6.92	50.45
	M0.8@S0.75	10.50	6.68	33.85
	M1.0@S0.25	4.03	7.31	103.44
	M1.0@S0.5	6.45	6.91	46.65
	M1.0@S0.75	10.94	6.79	27.97
SS	M0.5@S0.25	1.21	*	*
	M0.5@S0.5	1.38	*	*
	M0.5@S0.75	1.54	*	*
	M0.8@S0.25	1.29	*	*
	M0.8@S0.5	1.40	*	*
	M0.8@S0.75	1.54	*	*
	M1.0@S0.25	1.36	*	*
	M1.0@S0.5	1.47	*	*
	M1.0@S0.75	1.68	*	*
VFS		3.36	5.94	*
		5.38	6.36	*
		10.08	6.61	*
		3.55	7.56	*
		5.86	8.23	*
		10.59	8.46	*
		4.00	6.57	*
		6.40	7.30	*
		10.97	9.38	*

During the preparation of the Pickering emulsion, firstly, with the assistance of ultrasound (SB 3200D, Ningbo Xinzhi Biotechnology Co., Ltd), a selected amount of SiO_2 particles was dispersed in ethyl acetate at 20 kHz for about 5 min. Then, the deionized water was added into the ethyl acetate phase containing SiO_2 particles, which was mixed vigorously with a vortex mixer (IKA T25 digital Ultra Turrax, S25N-18G, German), set at a speed of 13,500 rpm for about 4 min. Finally, the obtained W/O Pickering emulsion was analyzed to characterize their morphology and

microstructure through visualization using an inverted microscope (Olympus IX73P2F, Japan) equipped with a 20× magnification of and a high speed digital camera (Phantom Miro R311, USA).

The suspension solution was prepared by mixing the same amount of modified SiO_2 particles with ethyl acetate assisted by ultrasound. The comparison of the Pickering emulsion and the suspension solution was carried out to validate the stability and the feasibility of the PES. The PES was also regarded as three-phase system, which included the modified SiO_2 particles, deionized water and ethyl acetate. A small amount of Sudan III was added into the emulsion phase to enhance visualization.

The experimental setup is schematically depicted in Fig. 1(a). The microchannel chip is a rectangle of 50 mm × 60 mm, the full-length of main channel is 167 mm, the cross section of the channel is an approximate square shape of 0.3 mm × 0.3 mm. The immiscible liquid-liquid two-phase fluids were introduced into the horizontal T-junction microchannel by two syringe pumps (Harvard 11 ELITE Single, USA) equipped with 10 mL syringes, respectively. A stereo microscope (Olympuss ZX2-ILLK, Japan) and a high speed digital camera (Phantom Miro R311, USA) were used to visualize two-phase flow patterns. The frame rates were set in the range of 3,200~10,000 fps (frames per second).

Fig. 1(b)&(c) illustrates the structure design and geometry of the microchannel reactor, where the continuous phase and the dispersed phase entered into two inlets, respectively. The microchannel reactor was made of quartz glass and sealed by a

thermal bonding method, fabricated by Suzhou Paifimeng Trading GmbH. Because of the strong hydrophilicity of the glass, the microchannel reactor was saturated initially with deionized water. During experiments, the volumetric flow rates of the dispersed phase and the continuous phase were set in the range of $10<Q_d<200$ μL/min and $10<Q_c<1300$ μL/min, respectively. The flow patterns were monitored at the T-junction regions with recorded snapshots and videos. The slug/droplet length was measured and averaged from at least 10 snapshots. In this work, *Re* and *Ca* for the continuous phase were in the ranges of 0.608~114.85 and 8.0×10^{-5}~0.05, respectively. After each experiment, the microchannels were cleaned by injecting acetone, acetic acid, and deionized water to remove residual chemicals, and finally dried ready for the next experiment.

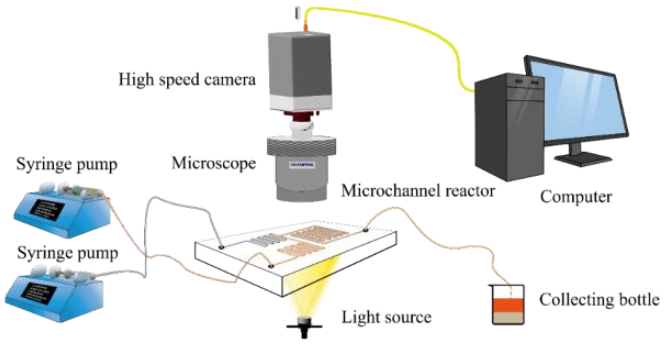

(a)

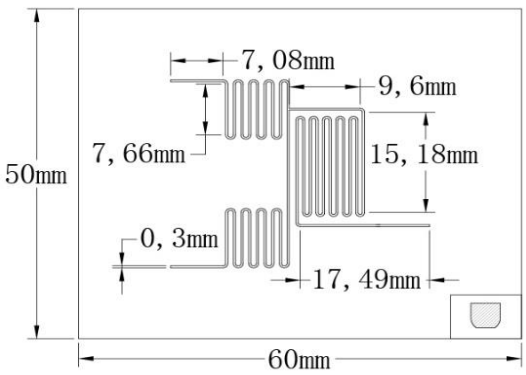

(b)

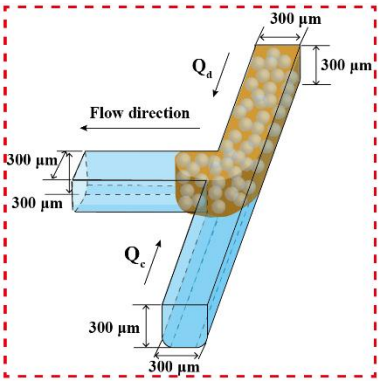

(c)

Fig. 1. (a) Schematic of experimental setup; (b) Layout design of microchannel reactor; (c) Schematic of the microchannel T-junction, 300 μm × 300 μm

3. Results and discussion

3.1 Characterization of the Pickering emulsions

The hydrophobicity of the surface of the modified SiO_2 nanoparticles was characterized by measuring contact angles of water droplets on the film coated with SiO_2 nanoparticles. The measurements (Fig. 2) showed that the contact angles increased from 18° of raw particles (M0.0) to 101° (M0.5), 127° (M0.8) and 143.3° (M1.0) as modified by a silane coupling agent methyltrimethoxysilane, respectively. As the amount of the silane coupling agent increased, the surface properties of SiO_2 nanoparticles switched from hydrophilicity to hydrophobicity, allowing to facilitate the formation of the W/O Pickering emulsion (Meng et al., 2020).

(a) (b) (c) (d)

Fig. 2. Contact angles of (a) raw (M0.0) and modified SiO_2 nanoparticles (dia. 20 nm) of (b) M0.5, (c) M0.8 and (d) M1.0

To examine the effect of the addition of SiO_2 nanoparticles on the emulsion droplet diameter, different amount of the modified SiO_2 nanoparticles with varying hydrophobicity were used. The results are shown in Fig. 3 and Table 1. As can be seen, increasing amount of SiO_2 nanoparticles resulted in reduction of the diameter of the dispersed droplets, but enhancement of the stability. For this system, the increase in SiO_2 nanoparticles amount improved the surface coverage, which decreased the

formed emulsion droplet size. This was likely due to the formation of a 3D network structure around the emulsion droplets that enhanced the stability of the Pickering emulsion (Binks et al., 2010). Binks' group (Aveyard et al., 2003) systematically studied the influence of SiO_2 particles concentration on the droplet size of Pickering emulsion system. They found that in a low particle concentration range (lower than 3%), the droplet size of the emulsion would decrease with increasing particle concentration. In this work, the concentration of SiO_2 particles is in the range of 2-6%. A 10-fold increase in particle concentration reduced the droplet size to about 1/8 of the original. That was overall well in line with the previous observation (Binks et al., 2004, 2005; Liu et al., 2012).

When the concentration of particles was higher than 3%, the droplet size would not change with the increase in particle concentration, and the extra particles tended to disperse in the continuous phase, not adsorb at the droplet interface. The stabilization mechanism is that the increase of the addition amount of solid particles means that the increase of the number of solid particles adsorbed at the oil-water interface, which leads to the thickening of the interface film, the enhancement of the ability to prevent the coalescence between droplets. In addition, coalescence is inhibited by the excess of particles because they enter oil phase and form a three-dimensional network, which increases the distance between droplets and stability (Binks et al., 2010).

As the amount of particles adsorbed on the oil-water interface increased, the oil-water interfacial tension decreased while a dense interface film formed, which effectively prevented the collision and the coalescence between the emulsion droplets.

Although the hydrophobicity of SiO_2 was in favor of the formation of the W/O Pickering emulsions, it had insignificant effect on the diameter of the droplets, that may be associated with a combination of a number of factors such as the non-spherical structure, the size distribution and the surface roughness of SiO_2 particles (Binks et al., 2000; Binks et al., 2005; Wu and Ma, 2016) (Fig. 3).

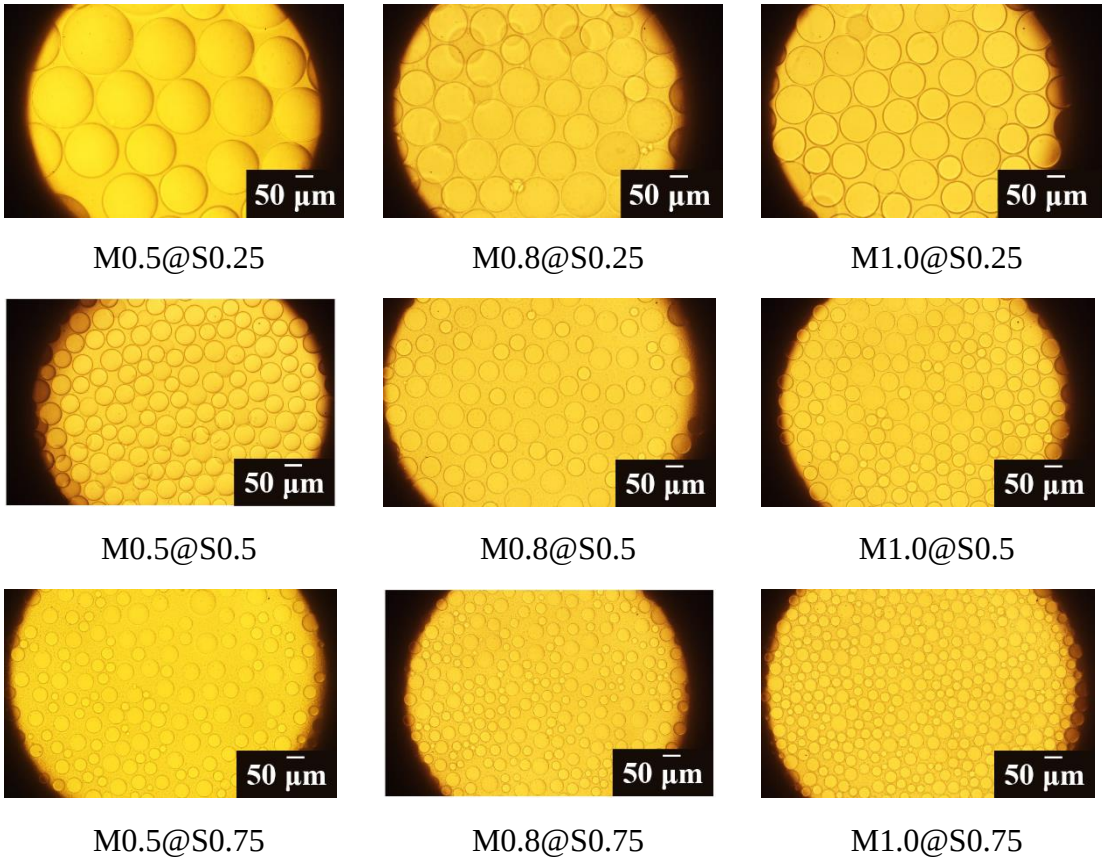

Fig. 3. Microscope image of Pickering emulsion droplets

3.2 Two-phase flow patterns of three systems of PES, SS and VFS

When the PES contains high-solid content and dispersed emulsion droplets, the apparent viscosity and density are generally high, exhibiting similar characteristics to fluids having high viscosity (Yao et al., 2018; Archibong-Eso et al., 2019; Wang et al., 2021). In order to identify the suitable operational parameters for achieving stable Pickering emulsion flow within microchannels, the prepared three multiphase flow

systems, i.e. PES, SS and VFS, were examined and compared. It is worth to note that the high viscous fluid was used as the dispersed phase in those three systems, which has been less studied previously (Cubaud and Mason, 2008; Bai et al., 2016; Zhang et al., 2019).

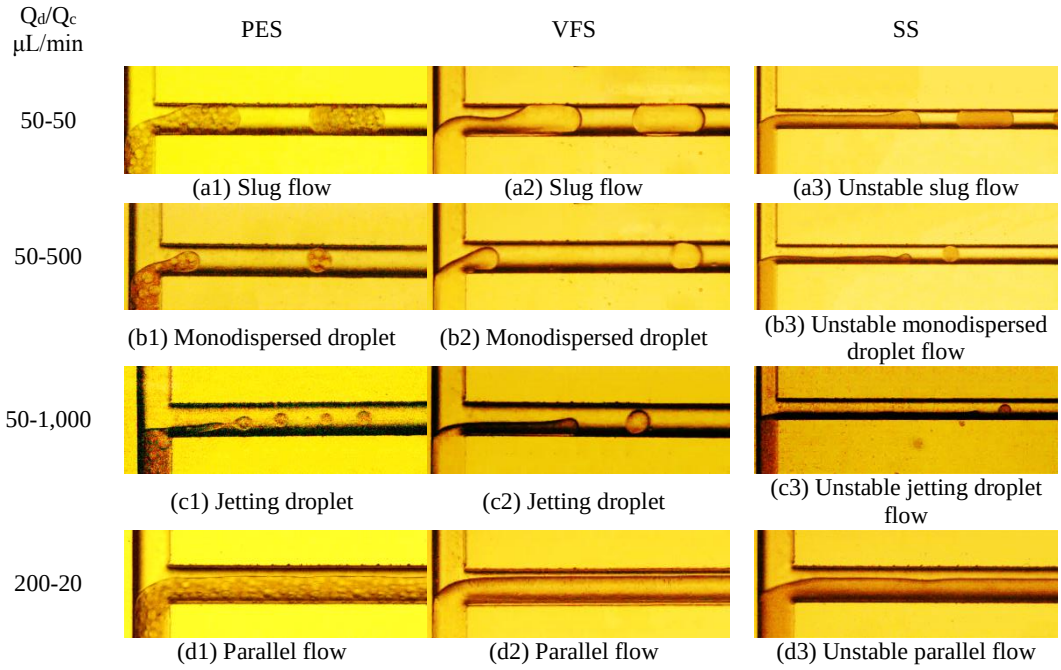

Fig. 4. Flow patterns observed around T-junction for three systems of PEs, SS and VFS

Fig. 4 illustrates the observed flow patterns with images covering the microchannel section across 20 mm downstream of the T-junction to allow the flow to fully develop. Four categories of stable flow patterns were observed for PES and VFS having comparable viscosities, namely, slug flow, monodispersed droplet flow, jetting droplet flow and parallel flow (Fig. 4). In these systems, the demulsification phenomena of Pickering emulsion in microchannel were not observed in all experiments. However, liquid-liquid two-phase immiscible flow patterns for SS were unstable, where the solid content of SS was identical with that of PES. These were similar to the previous observations, e.g. during the formation of other viscous droplets (Cubaud and Mason,

2008). In general, the formation of any specific flow pattern is a combination of many factors in the complex multiphase system under dynamic fluidic conditions, including fluid properties, fluidic operating parameters, and microchannel geometry/surface properties. The forces involved during the formation of dispersed droplets are further analyzed in the next Section.

For SS, the aqueous phase in the dispersed Pickering emulsion phase was replaced by ethyl acetate with the same volume. Fig. 5(a) shows that the suspension stretched along and attached to the channel wall when leaving the T-junction. Therefore, it was difficult to cut off the neck of the dispersed suspension phase at the T-junction. Fig. 5(b) shows that the dispersed droplets were formed at around the first bend of the main channel after flowing over a longer distance along the flow direction compared to PES, which was largely induced by Rayleigh-Taylor instability (Vadivukkarasan, et al., 2020). However, the dispersed droplets still tended to attach to the channel wall, which made the interface being elongated and deformed, even blocking the channel and finally forming some unstable flow patterns, as shown in Fig. 5(c).

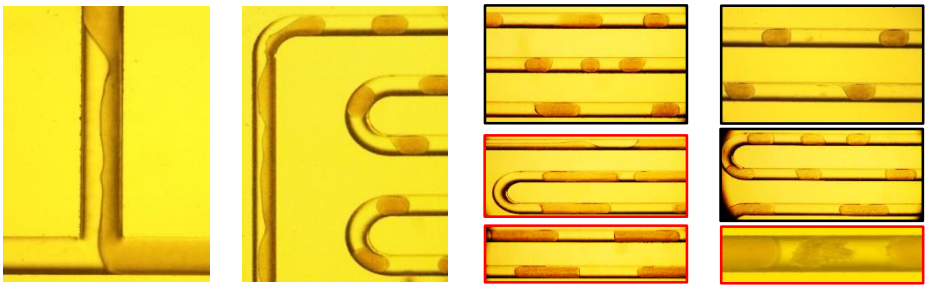

Fig. 5. Flow patterns of SS at different positions in microchannel (a) Around T-junction; (b) Around the bends of the microchannel; (c) In the main microchannel

For VFS, silicone oil was used to regulate the viscosity of ethyl acetate (oil phase),

in order to obtain comparable viscosities to that of the Pickering emulsion. The flow patterns and their formation processes are shown in Fig. 6. Four distinct flow patterns were also observed similar to that of PES, i.e. slug flow, monodispersed droplet flow, jetting droplet flow and parallel flow. These flow patterns were mainly formed by squeezing, dripping and jetting regimes, in accordance with observations in previous investigation with VFS by Yao et al. (2018) and Bai et al. (2016). In this work, the viscosity of PES increased with the increase in the addition amount of SiO_2 nanoparticles. In order to further clarify the influence of the dispersed W/S/O spherical emulsion droplets ($Ph_{2\text{-}1}$) on the formation of the dispersed Pickering emulsion phase, the introduction of VFS as a benchmark with the same viscosity should be important and necessary. For avoiding redundancy of the description about well known VFS, we tried our best to only list part experimental results. As VFS was out of the main scope of the present work, more experimental results for VFS are shown in Supporting Information.

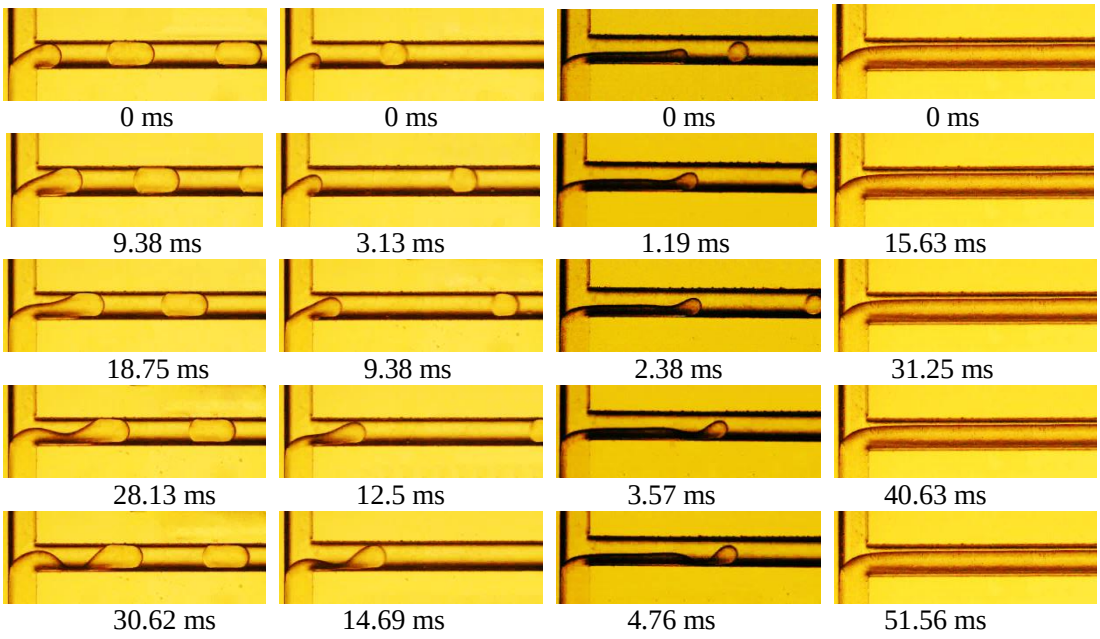

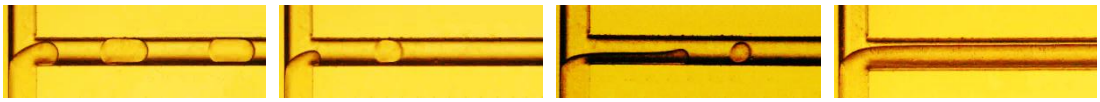

34.06 ms (a) 16.25 ms (b) 6.43 ms (c) 54.69 ms (d)

Fig. 6. Flow patterns and their formation processes for VFS. (a) Squeezing: Q_d=50 μL/min, Q_c=100 μL/min. (b) Dripping: Q_d=50 μL/min, Q_c=500 μL/min. (c) Jetting: Q_d=50 μL/min, Q_c=1000 μL/min. (d) Laminar: Q_d=200 μL/min, Q_c=20 μL/min

The above observed different flow patterns may have different effects on potential reaction applications involving Pickering emulsion, where both well-defined contact interface and the recirculation within the continuous phase or the dispersed phase exist. The former is conducive to the regulation of the reaction processes. The latter can significantly enhance local mixing leading to augmented heat and mass transfer (i) in the radial direction within the liquid slug, and (ii) in the axial dispersion across the gas-liquid interface, which is similar to the issues of gas-liquid two-phase systems (Kececi et al. 2009; Su et al. 2012). Therefore, Slug flow and Monodispersed droplet flow are believed to be more favourable for potential reaction applications.

3.3 Formation mechanism of PES dispersed droplets in microchannel

As discussed above, the PES was composed of a continuous water phase (Ph_1) and a dispersed Pickering emulsion phase (Ph_2), where the formation of the dispersed droplets was the result of a number of forces exerted upon the emerging droplet (Pickering emulsion). Fig. 7 illustrates those forces, including the inertia force caused by Ph_1 ($F_c \propto d_H^2 u_{WS}^2 \rho_W$) and by Ph_2 ($F_d \propto d_H^2 u_{PS}^2 \rho_P$), the interfacial force at the neck of Ph_2 ($F_\gamma \propto \gamma_{W/P} \delta_{neck}$), the viscous shearing force ($F_\mu \propto \mu_W Q_W L_D / \delta_{gap}^2$) caused by the flow of Ph_1 around the emerging droplet, the continuous phase pressure on the neck

(P_{neck}) and the tip (P_{tip}) of Ph_2 (Fig. 7).

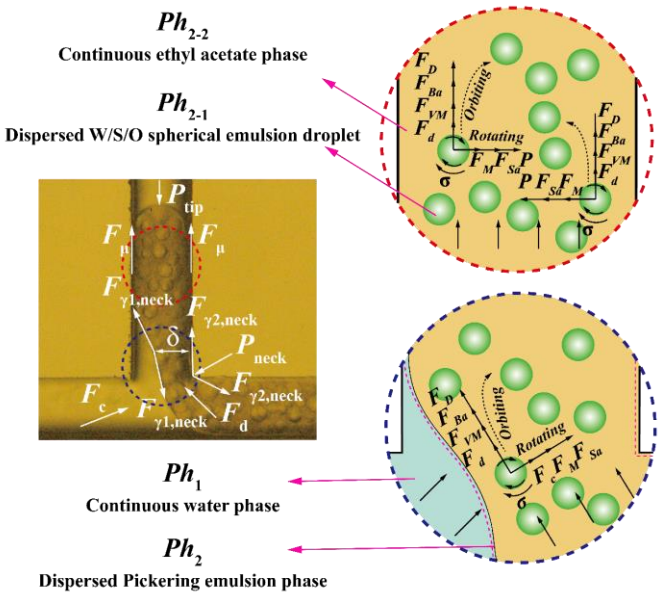

Fig. 7. Correlative forces for the formation of the dispersed droplets

The formation of the dispersed droplets was also believed to be the result of the dynamic competition among these forces. Specifically, as shown in Fig. 7, F_c and F_d were the main forces to drive Ph_2 to the downstream of the channel. F_μ also promoted the tip of Ph_2 towards the downstream, and caused the neck of Ph_2 to be quickly cut off, accelerating the formation of droplets. In addition, F_γ played an important role on the balance and the stability of the emerging droplet. At the neck of the dispersed phase, F_γ was balanced with F_c, F_μ and P_{neck} to ensure the dispersed phase to flow downstream continuously. The interfacial force caused the tail of the next emerging droplet to retract as the dispersed droplet forms, and the flow got into the transiently stable state. The interfacial force at the tip of the emerging droplet was balanced with F_μ and P_{tip}, in addition to the environmental confinement in the case of microchannels, to keep it moving downstream.

On the other hand, the dispersed W/S/O spherical emulsion droplets ($Ph_{2\text{-}1}$) and the continuous ethyl acetate phase ($Ph_{2\text{-}2}$) formed Pickering emulsion, as shown in Fig. 7(b). $Ph_{2\text{-}1}$ may be considered as quasi-solid soft microspheres due to SiO_2 particles acting as solid surfactant, where its moving trail was determined commonly by the drag force ($F_D \propto C_D \rho_o \left(u_o - u_{Ph_{2\text{-}1}}\right)^2 A_{Ph_{2\text{-}1}}$) induced by a range of factors, including $Ph_{2\text{-}2}$, the interfacial tension at the S/O interface (σ), the confinement of the microchannel wall, Basset force (F_{Ba}), virtual mass force (F_{VM}), Magnus force (F_M), Saffman force (F_{Sa}), and the collision and the repulsion forces between the adjacent emulsion droplets. The formation of the dispersed droplets was affected by the motion of $Ph_{2\text{-}1}$ in Ph_2, which depended on the size of $Ph_{2\text{-}1}$. The diameter of the dispersed droplets could be controlled by changing the addition amount of SiO_2 nanoparticles, and the dispersed phase neck formed with small size of $Ph_{2\text{-}1}$ was narrow. In addition, the small size of $Ph_{2\text{-}1}$ had a smaller torque, which increased the particle rotation speed, reduced the parabolic radian of motion, weakened the effect of F_D, accelerated the contract of neck, and led to the decrease of the size of the dispersed droplet.

The motion behaviors of $Ph_{2\text{-}1}$ in Ph_2 can be characterized over two regions, i.e. at the T-junction and in the main microchannel, as shown in Fig. 7(a). As the tip of the emerging Ph_2 began to intrude into the main channel at the T-junction, torque of $Ph_{2\text{-}1}$ occured under the action of F_c , F_d and F_D. The rotating motion was verified by an approximate clockwise direction. $Ph_{2\text{-}1}$ moved to the center of the microchannel due to F_M and F_{Sa}. Generally, the motion trajectory was more complex at the vicinity of T-junction due to the location distribution of $Ph_{2\text{-}1}$. Once the tip intruded into the main

channel, the streamline of all $Ph_{2\text{-}1}$ was almost identical and their vector direction was the same with F_{μ}, the disappearance of the rotation of $Ph_{2\text{-}1}$, F_M and F_{Sa}, so flow field was close to be stable and the motion trajectory showd a straight line (Fig. 7(b)).

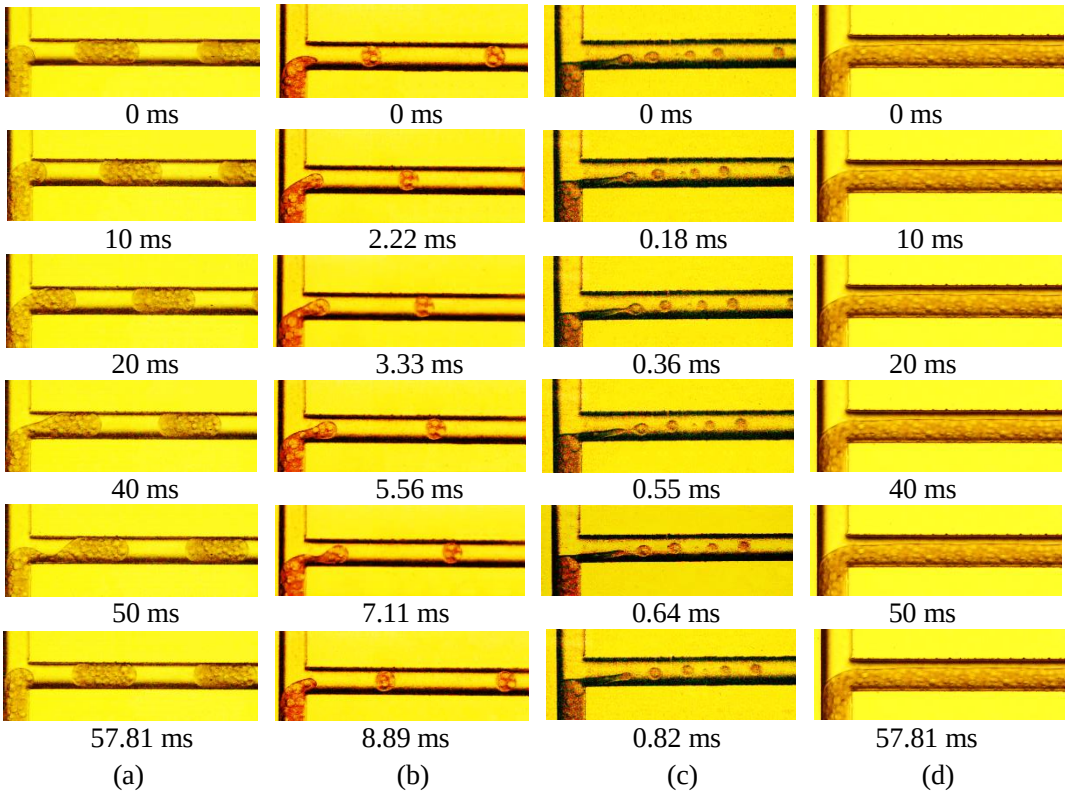

Fig. 8. Formation of the dispersed droplet for PES

(a) Squeezing, Q_d=50 μL/min, Q_c=50 μL/min; (b) Dripping, Q_d=50 μL/min, Q_c=500 μL/min; (c) Jetting, Q_d=50 μL/min, Q_c=1000 μL/min; (d) Laminar: Q_d=200 μL/min, Q_c=20 μL/min

Whilst the above analyzed forces affected the formation of Pickering emulsion droplets, they also influenced the overall multiphase flow behavior along the microchannel, forming different flow patterns under certain fluidic conditions (Fig. 4). Fig. 8 depicts the experimental observation captured during the formation of slug flow, monodispersed droplet flow and jetting droplet flow, by taking M1.0@S0.75 Pickering emulsion as an example, as detailed below.

Fig. 8(a) shows the dynamic formation of slug flow for PES at the T-junction in the

microchannel. The length of Pickering emulsion slugs was larger than the microchannel width. These slugs flowed along the channel, and were segmented from each other by the liquid plugs of Ph_1. Moreover, a thin continuous phase liquid film was located between the slug and the wall. This flow pattern was observed at a low Ph_1 flow rate (50 mL/min) and a 1:1 flow rate ratio of Ph_2 to Ph_1. In addition, the formation process of slug flow conformed to the squeezing mechanism. At the beginning of Ph_2 growth stage, the growth direction was perpendicular to the flow direction of the continuous phase in the main channel, and F_γ was dominant. Also, the size and the amount of $Ph_{2\text{-}1}$ had important influence on the formation and the width of the neck of the Ph_2 (Pan et al., 2018). Subsequently, Ph_2 gradually expanded at the inlet T-junction until blocking the main channel from time 0 ms to time 10 ms. The continuous phase flowed through the gap between Ph_2 and the channel wall, where the velocity of the continuous phase increased, as well as F_μ.

Fig. 9 schematically shows further analysis on the motion trajectory of $Ph_{2\text{-}1}$ in Ph_2, based on the observation captured by videos. It was found that $Ph_{2\text{-}1}$ on both sides of Ph_2 near the channel wall moved faster and migrated to the center of the channel (SI, Fig. S1). This was likely associated with $Ph_{2\text{-}1}$ around the tip tending to move clockwise as the torque induced the combined action of F_c, F_d and F_D. In the squeezing stage, the tip of Ph_2 continued to grow downstream under the balance with F_c, F_γ and P_{neck}, while the width of the neck of Pickering emulsion gradually decreased from time 10 ms to time 50 ms. At time 50 ms, the two-phase interface at the neck of the dispersed phase became a concave shape, which was similar to that of

high viscous fluid as the dispersed phase (Bai et al., 2016). Finally, the neck of the dispersed phase collapsed at time 52.81 ms. When the tail of the formed Pickering emulsion slug and the head of the new droplet quickly retracted due to the interfacial tension, the process entered into next squeezing period.

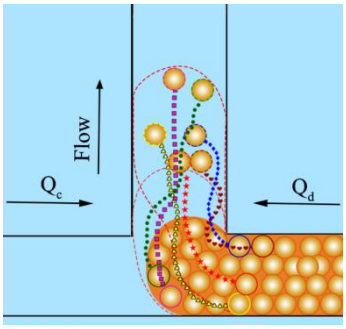

Fig. 9. Diagram of the motion trajectory of $Ph_{2\text{-}1}$ in Ph_2 (Q_c= Q_d=50 μL/min)

When the ratio of two-phase flow rate was relatively low (0.03~0.24), monodispersed drop flow and jetting droplet flow patterns were observed (Fig. 8 (b)&(c)), where higher continuous phase flow rates were favorable for forming jetting droplet flow. The formation of monodispersed droplets corresponded to the dripping mechanism. As the tip of the dispersed phase was unable to block the main channel due to the high continuous phase flow rate, it had to flow downstream under the strong push of F_μ and F_c. At the growth stage, the dispersed W/S/W/O spherical emulsion droplets entered into the tip of the dispersed phase, which expanded axially and radically, for example, from time 0 ms to time 3.33 ms. At the rupture stage, the neck of the dispersed phase began to gradually become narrower and slender, and only $Ph_{2\text{-}2}$ in Pickering emulsion can flow into the tip through the narrow neck, as seen from time 3.33 ms to time 8.89 ms in Fig. 8(b).

The length of the monodispersed droplet formed by the dripping mechanism was

smaller than the microchannel width because the shearing from the inertial or viscous force of the continuous phase was stronger than the two-phase interfacial tension. As the continuous phase flow rate continued to increase, Pickering emulsion phase was elongated and extended to downstream, thus the long narrow liquid column formed, which was pushed towards the center of the channel under the strong inertial force of the continuous phase (SI, Fig. S1). Due to the classical Rayleigh-Plateau instability (Xiao et al., 2016), the breakup of the tip of the Pickering emulsion occurred and small spherical droplets were formed at the moment of time 0.82 ms (Fig. 8(c)), i.e. the narrow liquid column was pinched off to form the jetting droplet flow.

When the flow rate ratio of dispersed phase to continuous phase was relatively high F_d began to dominate. As the dispersed phase cannot be cut off, it flowed side-by-side with the continuous phase in the microchannel (Fig. 8(d)). In this case, no dispersed droplets were formed, neither were slugs.

Overall, the diameter of Pickering emulsion droplets and the movement of $Ph_{2\text{-}1}$ were decisive factors for flow pattern and transition. With the decrease of SiO_2 amount, the diameter of emulsion droplets increased gradually, so δ was also relatively large that flow pattern transition needed larger j_c. When the diameter of the droplet was larger, the distribution became tighter, which led F_D increases on $Ph_{2\text{-}1}$, so the contraction of the neck of Ph_2 was inhibited, and the flow pattern transition lines were raised eventually.

3.4 Flow pattern maps for PES in microchannels

As discussed above, the formation of a specific flow pattern is determined by a

number of factors, including fluid properties and operating parameters, during the complex multiphase flow within a given microchannel. To identify suitable operating conditions in order to achieve a specific flow pattern, were varied the hydrophobicity of SiO_2 nanoparticles, the amount of SiO_2 nanoparticles added, and both phases' superficial flow velocities (j_d and j_c for dispersed and continuous phase, respectively). The properties and amounts of SiO_2 particles are specified in Table 1, while the two phases' superficial flow velocities, j_d and j_c, were operated in the range of j_d=0~40 mm/s and j_c=0~350 mm/s, respectively. Fig. 10 shows the flow pattern maps corresponding to those variables, with the transition curves dividing different flow pattern zones.

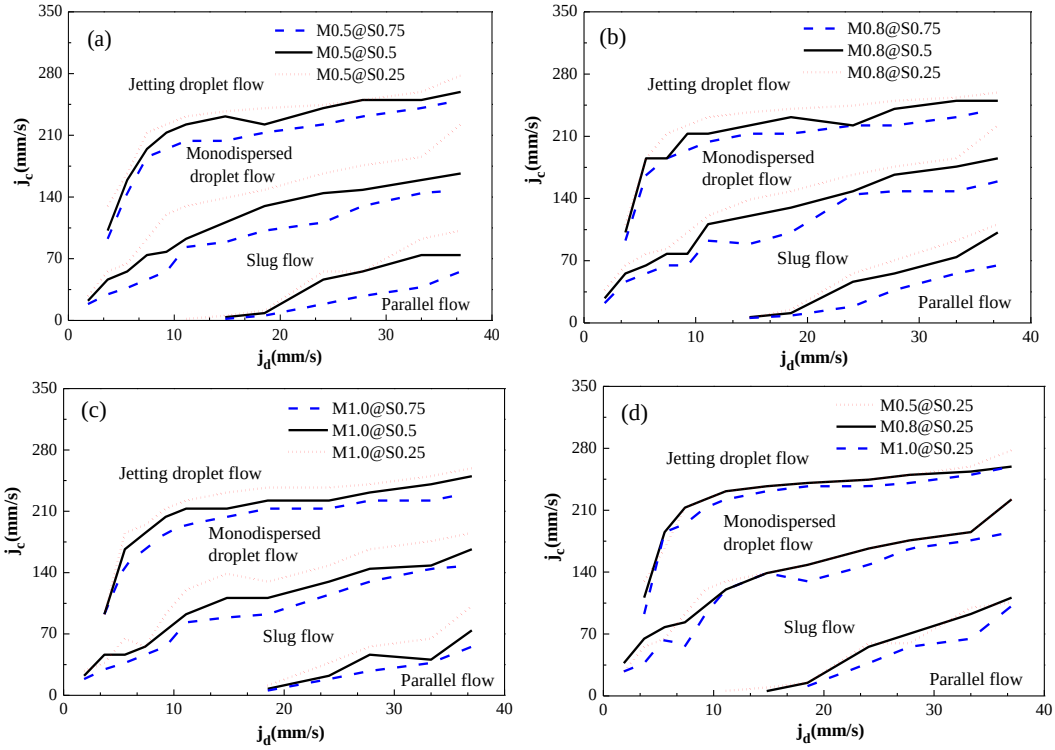

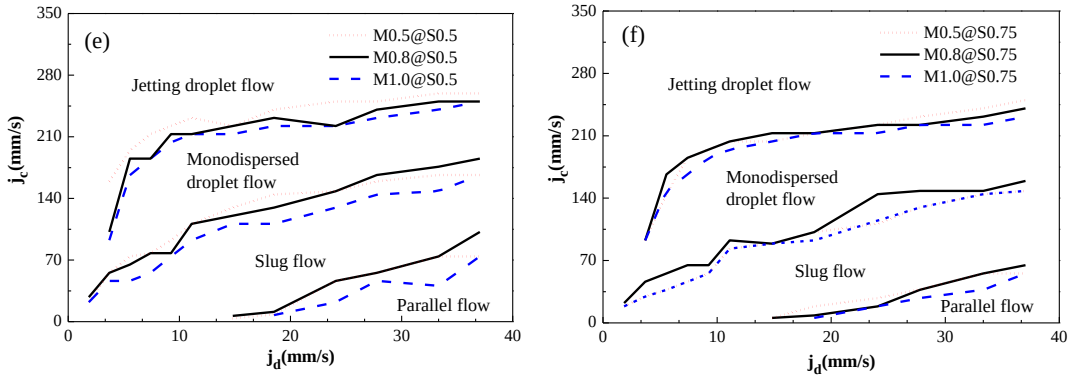

Fig. 10. Flow patterns and flow pattern transition lines for PES flow in microchannels with varying superficial velocities of dispersed phase and continuous phase, and amounts of methyltrimethoxysilane and SiO_2 nanoparticles

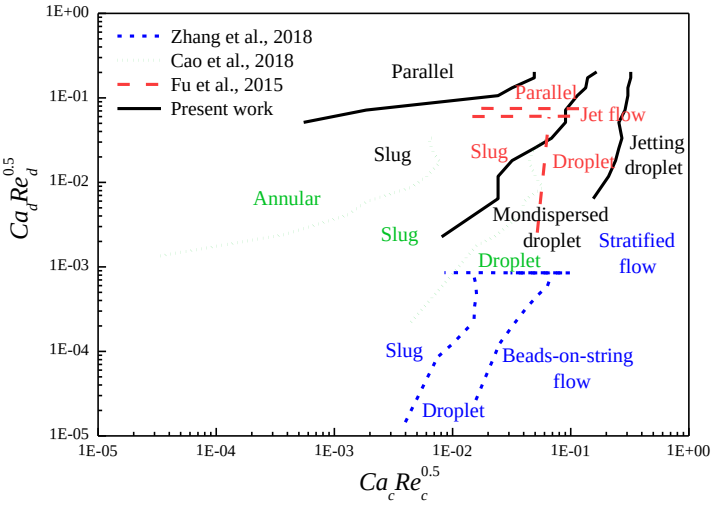

Fig.11. Comparison between the flow pattern map in the present study and that in the literature

As can be seen in Fig. 10(a), for a specific multiphase system increasing one phase's superficial velocity required to increase the other phase's velocity in order to realize a flow pattern transition. At a given j_d level, increasing j_c facilitated the transition from parallel flow, through slug flow and monodispersed drop flow, to jetting droplet flow. Clearly, the parallel flow zone occupies the smallest zone, located at the bottom right corner of the flow pattern map, requiring a higher flow rate ratio of Ph_2 to Ph_1 under high flow rates of Pickering emulsion. It was interesting to note that

those trends applied to all multiphase systems examined (Fig. 10(a)-(f)). Also, these observations were in line with that shown in Figs. 4 & 8.

For a given j_d, when increasing j_c, the flow pattern transited from parallel flow to stable slug flow, mainly due to the dominance of F_γ over F_c and F_μ. By further increasing j_c, the flow pattern changed from slug flow to monodispersed drop flow, finally to jetting droplet flow, while the shearing from large F_c or F_μ dominated over F_γ forming monodispersed drop flow and jetting droplet flow patterns. Compared to traditional liquid-liquid two-phase systems, the regions of the dispersed flow patterns (slug flow, monodispersed drop flow and jetting droplet flow) significantly increased (Zhao et al., 2006; Tsaoulidis et al., 2013; Cao et al., 2018; Yao et al., 2018). Also, the dispersed flow patterns easily formed with PES, which increased the feasibility of the solid conveying based on Pickering emulsion.

Regarding effect of added SiO_2 amount, Fig. 10(a)-(c) show that the decrease of SiO_2 amount, for a selected amount of methyltrimethoxysilane at a given j_d level, shifted upwards all the transitions curves requiring higher j_c, i.e. the smaller amount of SiO_2 added, the higher j_c, needed. This may be explained by the decrease of viscosity and two-phase interfacial tension, and the increase of diameter of the dispersed emulsion droplets in Pickering emulsion, given a decreased amount of SiO_2 nanoparticles added. During the formation of the dispersed emulsion droplet, the size of $Ph_{2\text{-}1}$ affected the break-up of the neck except for the balance between the shear stress and the interfacial tension according to our experimental observation. Moreover, the larger the $Ph_{2\text{-}1}$ size was, the stronger the impediment for the break-up of the neck

was. The effects of the amount of methyltrimethoxysilane, i.e., the hydrophobicity of SiO_2 nanoparticle surface on flow patterns are illustrated in Fig. 10(d)-(f), showing insignificant influence. This was mainly due to the variation of the Pickering emulsion droplet diameter to be insignificant with the increase of the methyltrimethoxysilane amount for a given amounts of SiO_2 nanoparticle, as shown in Figs. 3. For S0.25, with the increase of methyltrimethoxysilane amount, the critical velocity of Pickering emulsion for forming parallel flow gradually increased, which may be caused by the larger Pickering emulsion droplet diameter, as shown in Figs. 3 & 10(d). This was a typical situation where F_d or F_μ dominated over F_γ.

Fig. 11 shows the comparison between results from the present study and those in the literature. Based on the above discussion, key factors including viscosity, interfacial tension, two-phase velocity, characteristic scale of Pickering emulsion droplets and its motion of $Ph_{2\text{-}1}$ in Ph_2 all play an important role in the formation of the flow patterns, and further in the flow pattern transition boundary on the flow pattern map. Therefore, the composite dimensionless numbers were adopted to plot the flow pattern map, which were also employed previously (Yagodnitsyna et al., 2016; Yao et al., 2018).

As seen in the map, overall the central zone of the flow pattern map was occupied by the slug flow, which belonged to the interfacial tension dominated zone and the squeezing regime. The slug-droplet transition line in the present experiment shifted to top-left in the map compared to the traditional two-phase system (Cao et al., 2018; Zhang et al., 2018). This was attributed to larger interfacial tension and viscosity of the dispersed phase for PES, which postponed the occurrence of the dispersed droplets. Moreover, the trends of almost all the transition lines were similar. It indicated that the results from traditional high viscous systems could be extrapolated to PES in the microchannel.

By increasing the velocity or viscosity of the dispersed phase for traditional

systems, the parallel flow was prone to be formed under the domination of the dispersed inertia or viscous force. The viscosity of Ph_2 for PES increased with the increase in the solid content, whilst the diameter of $Ph_{2\text{-}1}$ reduced. Further, the neck width of the dispersed phase at the T-junction became narrower, which was unfavorable for the formation of the parallel flow. Other transition lines in the cyclohexane-CMC two-phase flow in rectangular microchannels were almost vertical (Fu et al., 2015), which were different from the present observation. That was likely due to the interfacial tension of their system being remarkably large (37 mN/m), which led to the increase of the interfacial tension dominated zone.

3.5 The length of the dispersed droplets in PES, SS and VFS

Upon establishment of a stable state for the formation of Pickering emulsion dispersed droplets, it is also important to characterize and, ultimately, achieve the desired droplet geometry. Within a confined microchannel, the dimensionless number L_D/w (i.e., length of dispersed phase droplet/width of microchannel) represents a characteristic quantity to describe the physical geometry of droplets under flow. Fig. 12(a)-(c) plot the variation of L_D/w as a function of total flow rate (Q_t) at a constant flow rate ratio of Q_d/Q_c = 1:1 for the PES flowing along the main microchannel. Different amounts of SiO_2 particles (0.25 g, 0.50 g and 0.75 g) with varying hydrophobicity (by adding 0.5 mL, 0.8 mL and 1.0 mL silane coupling agent) were employed. For comparison, an SS flow system was examined under the identical operating conditions (Fig. 12(d)-(f)). A wider range of operating conditions was also applied and the experimental results together with flow patterns observed are presented in Supporting Information (SI, Figs. S2-S3).

As can be seen in Fig. 12(a) for the PES, L_D/w decreased with the increase of total

two-phase flow rate for all three amounts SiO_2 addition, while the increase of modified SiO_2 addition resulted in the decrease in L_D/w. With the increase of SiO_2 amount, the diameter of emulsion droplet decreased, which was conducive to the contraction of the neck width of the dispersed phase (δ), and accelerated the droplet fracture under the same operating conditions. By increasing hydrophobicity following more silane coupling agent added from 0.5 mL to 1.0 mL (Fig. 12(a)-(c)), L_D/w was reduced correspondingly. As the two-phase interfacial tension almost kept constant with the increase of the amount of SiO_2, its effects on the the droplet length could be negligible. On the other hand, the increase of SiO_2 amount was in favor of the decrease of the neck width of the dispersed phase at the T-junction, potentially leading to decrease of the size of the emulsion droplet in Ph_2 and, in turn, decrease in L_D/w.

For the SS flow under identical operating conditions (Fig. 12(d)-(f)), it showed a similar trend in terms of L_D/w as a function of total flow rate, where L_D/w was generally larger than that of PES. More significantly, all SS flows appeared to be very unstable without obvious regularity, which was largely due to the adhesion of solid particles on the channel wall (Fig. 5). It was found that the solid particles in the suspension were easy to deposit at the bottom and adhere to the microchannel in SS, resulting in channel blockage. The solid particles in the suspension were easy to deposit under the action of gravity (F_G), which finally entered the water phase from the oil phase due to the drag force (F_D) produced by its own adhesion channel. This was a typical F_D dominated interfacial tension (F_γ).

Meanwhile, the comparison of the dispersed droplet length of VFS and PES is

depicted in Fig. 13. The experimental results showed that the length decreased with the increase of the dispersed phase viscosity for a given Q_d/Q_c, and it was in accordance with the literature reports (Bai et al., 2016). It was also found that the length for VFS was clearly larger than PES under the identical operating conditions, and the difference was induced by the emulsion droplet in Ph_2. The experimental results for other operating conditions are shown in SI, Fig. S4-S5.

On the one hand, there were little differences in both two-phase interfacial tension and viscosity between PES and VFS (Table 1), where their influence on the formation of the dispersed phase droplets was insignificant. With the increase of Ph_2 viscosity, meanwhile, the diameter of $Ph_{2\text{-}1}$ was smaller, which made the neck width of the dispersed phase decrease and F_μ become the dominant force, so the size of Ph_2 decreases. On the other hand, the existence of the emulsion droplets in Ph_2 promoted the break-up of the neck. Moreover, the smaller the diameter of the emulsion droplets was, the faster the collapsing velocity of the neck was. In order to elucidate the mechanism of the effects of the dispersed emulsion droplet in Ph_2, further study will be required, which is ongoing in our laboratory.

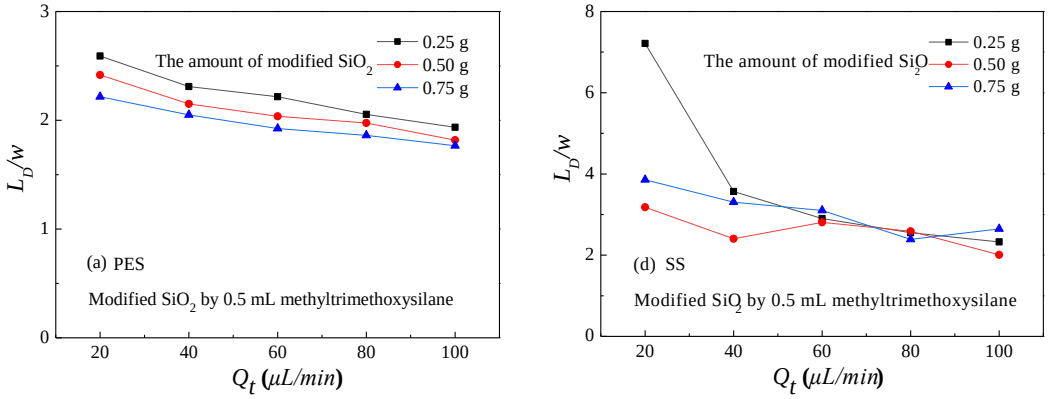

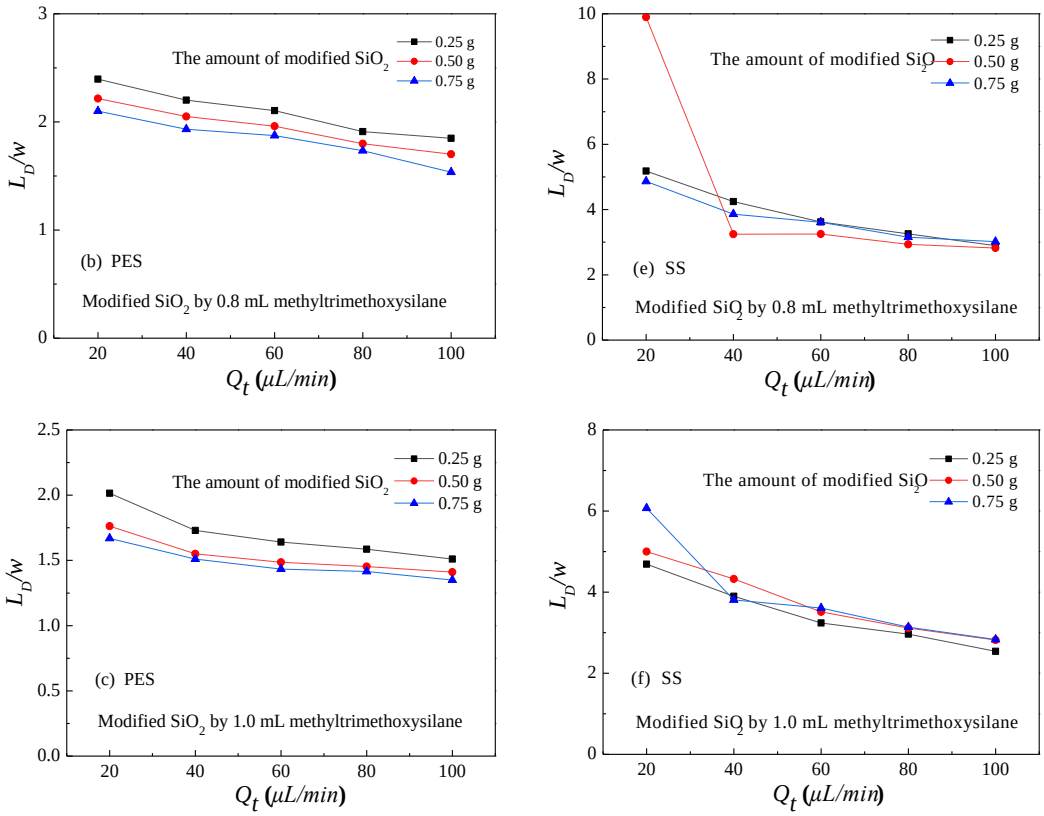

Fig. 12. Effects of the flow rate on length of dispersed phase droplets in PES (a-c) and SS (d-f) at a flow rate ratio of 1:1

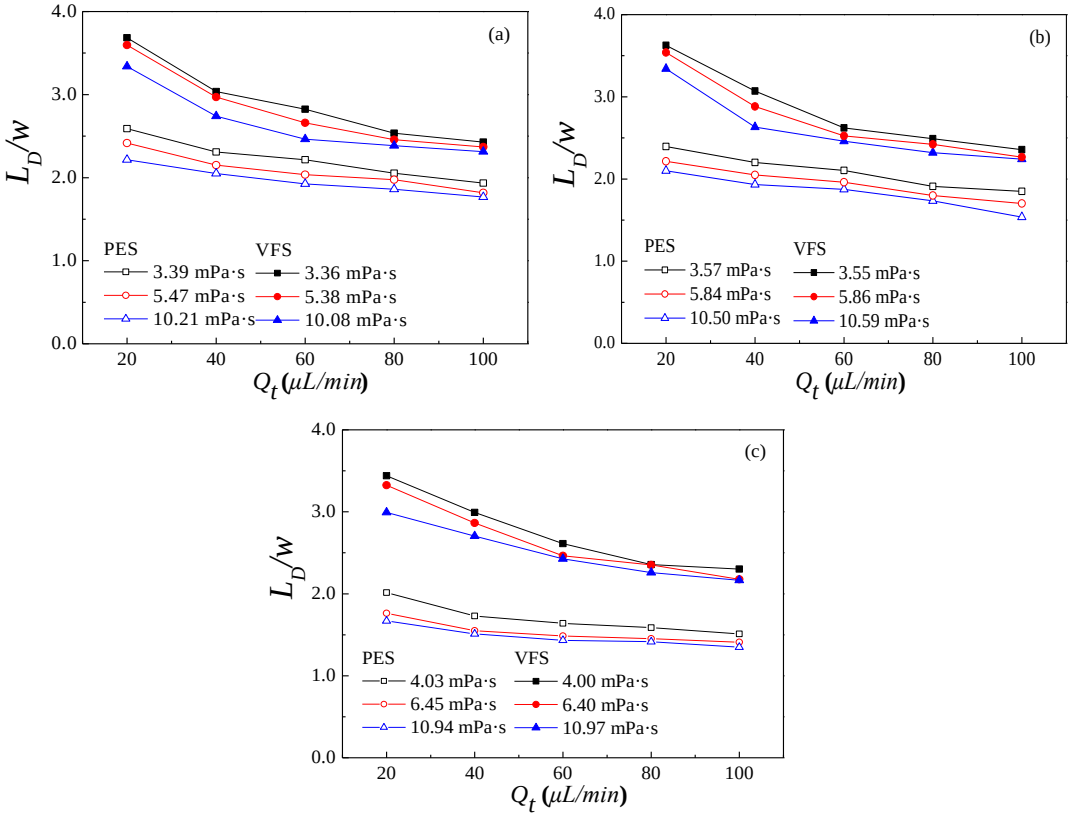

Fig. 13. Comparison of L_D/w of VFS and PES at a flow rate ratio of 1:1

3.6 Empirical correlation for the length of the dispersed droplet

It was interesting that the size of the dispersed W/S/O spherical emulsion droplets ($Ph_{2\text{-}1}$) played an important role on the formation of the dispersed Pickering emulsion phase (Ph_2). The possible reason was that the complicating movement of $Ph_{2\text{-}1}$ in Ph_2, the interaction between adjacent $Ph_{2\text{-}1}$, and the rigid shell of $Ph_{2\text{-}1}$ under the balance of all forces in the above discussion. Compared with conventional homogeneous dispersed phase, the dynamic behaviors of the dispersed Pickering emulsion made of $Ph_{2\text{-}1}$ and the continuous ethyl acetate phase ($Ph_{2\text{-}2}$) were more complex. Although many rational models based on classical Garstecki's scale law model have been proposed in the previous literatures for the squeezing regime (Garstecki et al., 2006; van Steijn et al., 2007; Leclerc et al., 2010; Xiong et al., 2007; Shao et al., 2008), the shearing regime (de Menech et al., 2008; Guo and Chen, 2009; Thorsen et al., 2001; Husny and Cooper-White, 2006; Xu et al., 2008) and the transition squeezing/shearing regime (Christopher et al., 2008; de Menech et al., 2008; Xu et al., 2008; Fu et al., 2010), these models were difficult to extrapolate to those complex systems involving internal movement in the dispersed phase-Pickering emulsion.

Considering the complexity of the movement of $Ph_{2\text{-}1}$ in Ph_2, moreover, our investigation for the application of Pickering emulsion in microchannels was only in the preliminary stage, so the rational model for predicting the length of the dispersed droplet (L_D/w) was difficult to be proposed. Based on the rule of thumb, the empirical correlation would be adopted in this work. Essentially, our proposed empirical

correlation still originated from classical Garstecki's scale law model. Meanwhile, several classical and latest models were introduced to compare with our empirical model and the experimental results, as shown in Fig. 15. It was obvious that the predicted values from previous models were rather larger than the experimental results. The main reason for the difference was the negative effects of $Ph_{2\text{-}1}$ on the break-up of the dispersed phase at the T-junction, that is, the existence of $Ph_{2\text{-}1}$ in Ph_2 impeded the formation of Ph_2. So, the viscosity ratio and *Ca* were adopted in the empirical correlation.

These slug droplets were formed under squeezing ($Ca<1.5\times10^{-3}$). The experimental results showed that the length of the dispersed droplet was affected by the viscosity ratio and *Ca*, and the change of the viscosity of Ph_2 affected the size and movement of $Ph_{2\text{-}1}$ in Ph_2. That is, the intrinsic mechanism of the above influence of fluid viscosity on droplet formation could be attributed to the external shear stress and the movement behavior of $Ph_{2\text{-}1}$ in Ph_2. So these two important dimensionless numbers were introduced on the basis of the prediction formula mentioned in the literature, the results showed that droplet size of all systems could be predicted well.

In order to establish a scaling law for the Pickering emulsion flow, an empirical correlation was developed for the flow characteristic number L_D/w with a wider range of fluidic parameters, by introducing two additional dimensionless numbers, $Ca=\mu_c u_c/\gamma$, and $\lambda=\mu_d/\mu_c$, based on the experimental investigations. Fig. 14 shows experimental results for L_D/w as a function of *Ca* at three levels of viscosity ratio (λ) with a given flow rate of the dispersed phase (Q_d) and hydrophobicity of SiO_2 particle

surface. The experimental results for a wider range of operating conditions are presented in SI (Figs. S6-S7).

As shown in Fig. 14(a), initially, L_D/w dropped sharply with the increase of Ca, followed by gradually leveling off as $Ca>1.5\times10^{-3}$. With given Q_d (20 μL/min) and λ, the increase in Ca reflected a higher flow rate of the continuous phase (Q_c), speeding up the contraction of the phase interface while reducing the detachment time of the droplet, finally leading to the decrease of L_D/w. For given Ca and Q_d, the decrease of λ resulted in increase of L_D/w, where the lower viscosity of the dispersed phase was in favor of the pinch-off of the neck while taking a shorter period of time to complete the formation of the dispersed droplet.

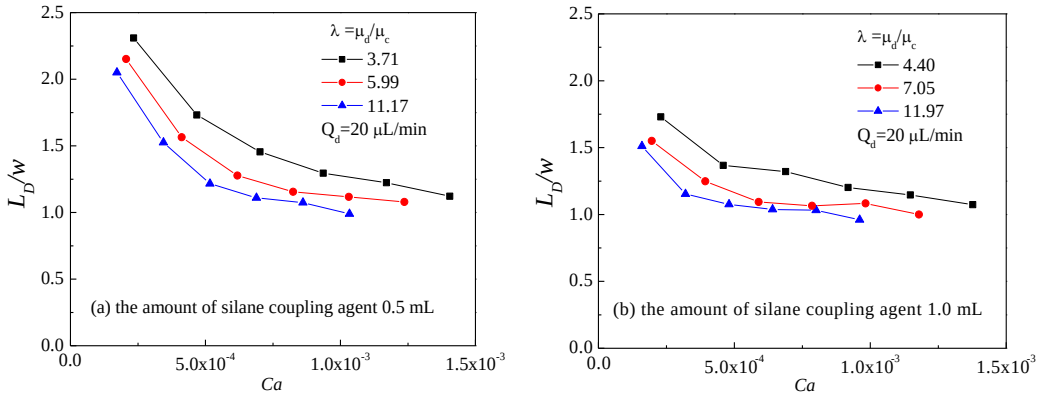

Fig. 14. L_D/w vs. Ca at different λ and SO_2 particle hydrophobicity levels with a given Q_d for PES

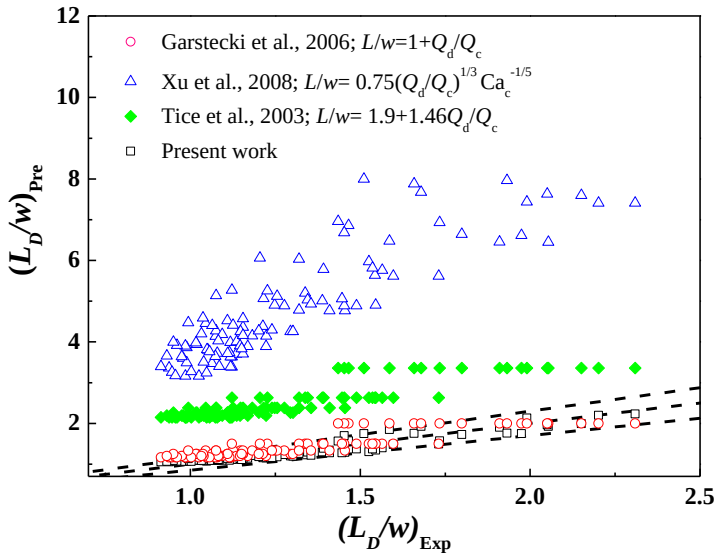

Fig. 15. Comparison of L_D/w between the fitting results from Eq. (1) and the references, $1.6\times10^{-4}<Ca<3.0\times10^{-3}$

As demonstrated above, the droplet length in terms of L_D/w was significantly influenced by viscosity and volumetric flow rates of the two phases, liquid properties and interfacial tension within a confined microchannel. Based on the experimental measurements, a scaling law was proposed for L_D/w by considering those key parameters. By using a multi-variable least squares method to fit all the experimental data, an empirical correlation was obtained (Eq. (1)). For comparison, an empirical correlation for VFS was also carried out (Eq. (2)). It was also interesting that the value of the exponents might be indicative of the influence of the leakage flow at the corner of microchannel, which may also be associated with the defects of the empirical correlation.

$$\text{PES:}\quad \frac{L_D}{w}=1+0.08\left(\frac{\mu_d}{\mu_c}\right)^{-0.56}\left(\frac{Q_d}{Q_c}\right)^{0.91}Ca^{-0.41} \tag{1}$$

$$\text{VFS:}\quad \frac{L_D}{w}=1+0.17\left(\frac{\mu_d}{\mu_c}\right)^{-0.36}\left(\frac{Q_d}{Q_c}\right)^{0.45}Ca^{-0.40} \tag{2}$$

The empirical correlations show that L_D/w is more dependent on Q_d/Q_c than Ca and λ for both PES and VFS. Compared to VFS, the effects of Q_d/Q_c and λ on L_D/w are larger for PES than VFS. Interestingly, Ca plays an almost equivalent role in influencing L_D/w for PES and VFS. The reason behind this phenomenon is worth investigating further.

The validation of the two correlation models, Eq. (1) & (2), was conducted by comparing the predicted values and experimental results of L_D/w (Fig. 16). It can be seen that the relative errors of the predictions for L_D/w all fall within ±15% for both PES and VFS. Considering the uncertainty associated with experimental quantification of L_D/w, the predicted values were in satisfactory agreement with the experimental data. These results indicated that the scaling law could be applied to predict L_D/w for droplet/slug flow in microfluidic T-junction with an acceptable accuracy.

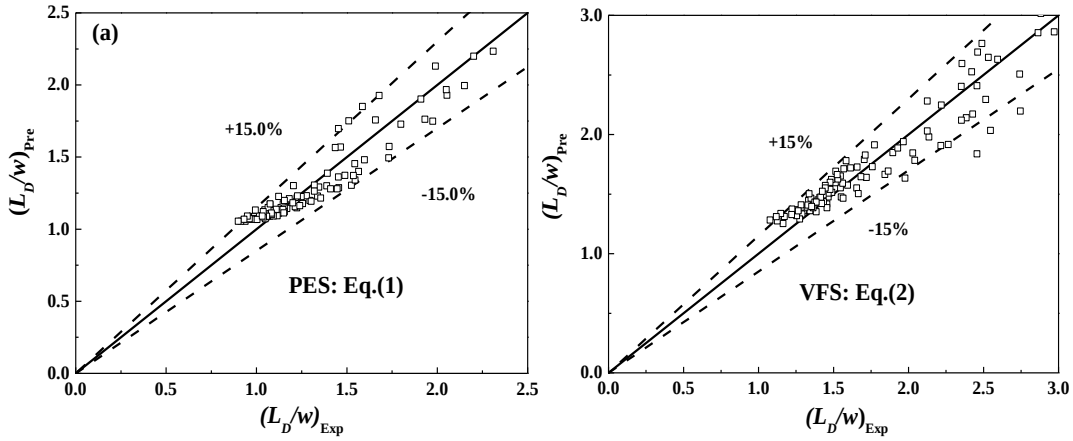

Fig. 16. Comparison of the predicted values and the experimental data for PES and VFS

4. Conclusion

The clogging and difficulties in achieving stable operation in multiphase flow involving solid micro/nano particles are still severe challenges for heterogeneous

catalytic reactions or other multiphase processes in microchannel reactors. To address those challenges, the Pickering emulsion was adopted in the present work. The microfluidic behavior and hydrodynamics of Pickering emulsion systems (PES) within a microchannel reactor were systematically characterized, both experimentally and theoretically, under a range of operating conditions. For comparison, a suspension system (SS) formed with ethyl acetate containing suspended SiO_2 nanoparticles and water, and a viscous fluid system (VFS) consisting of ethyl acetate, methyl-silicone oil and water, were also examined.

(1) Liquid-liquid two-phase flow hydrodynamics of PES, SS and VFS around the T-junction within the main microchannel were dependent on a range of parameters, including surface hydrophobicity of stabilizing SiO_2 nanoparticles, amount of SiO_2 particles added, viscosity and flow rate.

(2) Four flow patterns of parallel flow Slug flow, monodispersed droplet flow, and jetting droplet flow were observed under these operating conditions for PES and VFS, where superficial velocity was the key factor affecting the flow patterns transition. The dispersed droplets were prone to adhere to the channel wall for SS, which made the interface be elongated and deformed, even block the channel.

(3) The formation of slug flow was the result of the dynamic competition among the inertia force (F_c, F_d), the interfacial force (F_γ), the viscous shearing force (F_μ) and the continuous phase pressure (P_{neck}, P_{tip}).

(4) The motion behavior of interface $Ph_{2\text{-}1}$ was determined by drag force (F_D), interfacial tension at the S/O interface (σ), confinement of the microchannel wall,

Basset force (F_{Ba}), virtual mass force (F_{VM}), Magnus force (F_M), Saffman force (F_{Sa}), and collision and the repulsion forces between the adjacent emulsion droplets. The motion trajectory showed the characteristics of the approximate clockwise direction and the straight line.

(5) A scaling law of the droplet size (L_D/w) was developed as a function of Q_d/Q_c, μ_d/μ_c and Ca. The results showed that the predicted values were in accordance with the experimental data.

SUPPORTING INFORMATION

Experimental data under other operating conditions are shown in Supporting Information.

Acknowledgements

We gratefully acknowledge the financial supports from National Natural Science Foundation of China (Nos. 21978250, 21808194), Natural Science Foundation of Shandong Province (ZR2017BB058) and Key Technology Research and Development Program of Shandong (2019JZZY010410).

Nomenclature

$A_{Ph2\text{-}1}$	Cross-sectional area of $Ph_{2\text{-}1}$, m^2
Ca	Capillary number, $Ca=\mu_c u_c/\gamma$
C_D	Drag coefficient
d	Pickering emulsion droplet diameter, μm
d_H	Hydraulic diameter, m
F_{Ba}	Basset force, N
F_c	Inertia force caused by Ph_1, N
F_d	Inertia force caused by Ph_2, N
F_D	Drag force, N

F_M	Magnus force, N
F_{Sa}	Saffman force, N
F_{VM}	Virtual mass force, N
$F_{\gamma,\ neck}$	Interfacial force on the neck, N
F_μ	Viscous shearing force, N
j_c	Superficial velocity of the continuous phase, mm/s
j_d	Superficial velocity of the dispersed phase, mm/s
L_D	Length of the dispersed phase droplets, μm
M	Amount of methyltrimethoxysilane, mL
Ph_1	Continuous water phase
Ph_2	Dispersed Pickering emulsion phase
$Ph_{2\text{-}1}$	Dispersed W/S/O spherical emulsion droplets
$Ph_{2\text{-}2}$	Continuous ethyl acetate phase
P_{neck}	Continuous phase pressure on the neck of Ph_2, N/m^2
P_{tip}	Continuous phase pressure on the tip of Ph_2, N/m^2
Q_c	Flow rate of the continuous phase, μL/min
Q_d	Flow rate of the dispersed phase, μL/min
Q_t	Total flow rate of two phases, μL/min
$@S$	Amount of modified SiO_2, g
t	Time, ms
u	Superficial velocity, m/s
w	Microchannel width, μm
Greek letters	
γ	Interfacial tension, mN/m
δ_{neck}	Thickness of the emerging Ph_2 tip, m
δ_{gap}	Gap between the wall and the dispersed phase, m
μ	Dynamic viscosity, mPa·s
λ	Two-phase viscosity ratio, $\lambda=\mu_d/\mu_c$
ρ	Density, kg/m^3
σ	Interfacial tension at the S/O interface, mN/m

References

Abadie, T., Xuereb, C., Legendre, D., Aubin, J., 2013. Mixing and recirculation characteristics of gas-liquid Taylor flow in microreactors. Chem. Eng. Res. Des. 91, 2225-2234.

Adamo, A., Beingessner, R.L., Behnam, M., Chen, J., Jamison, T.F., Jensen, K.F., Monbaliu, J.C.M., Myerson, A.S., Revalor, E.M., Snead, D.R., Stelzer, T., Weeranoppanant, N., Wong, S.Y., Zhang, P., 2016. On-demand continuous-flow production of pharmaceuticals in a compact, reconfigurable system. Science 352, 61-67.

Archibong-Eso, A., Shi, J., Baba Y.D., Aliyu, A.M., Raji, Y.O., Yeung, H., 2019. High viscous oil-water two-phase flow: experiments and numerical simulations. Heat Mass Transfer 55, 755-767.

Aveyard, R., Binks, B.P., Clint, J.H., 2003. Emulsions stabilised solely by colloidal

particles. Adv. Colloid. Interface 100, 503-546.
Bai, L., Fu,Y.H., Zhao S.F., Cheng Y., 2016. Droplet formation in a microfluidic T-junction involving highly viscous fluid systems. Chem. Eng. Sci. 145, 141-148.
Binks, B.P., Lumsdon, S.O., 2000. Influence of particle wettability on the type and stability of surfactant-free emulsions. Langmuir 16, 8622-8631.
Binks, B.P., Lumsdon, S.O., 2001. Pickering emulsions stabilized by monodisperse latex particles: effects of particle size. Langmuir 17, 4540-4547.
Binks, B.P., Whitby, C.P., 2004. Silica particle-stabilised emulsions of silicone oil and water: aspects of emulsification. Langmuir. 20, 1130-1137.
Binks, B.P., Whitby, C.P., 2005. Nanoparticle silica-stabilised oil-in-water emulsions: improving emulsion stability. Colloid. Surface. A., 253, 105-115.
Binks, B.P., Fletcher, P.D.I., Holt, B.L., Kuc, O., Beaussoubre, P., Wong, K., 2010. Compositional ripening of particle-and surfactant-stabilised emulsions: a comparison. Phys. Chem. Chem. Phys. 12, 2219-2226.
Cao Z., Wu Z., Sundén, B., 2018. Dimensionless analysis on liquid-liquid flow patterns and scaling law on slug hydrodynamics in cross-junction microchannels. Chem. Eng. J. 344 604-615.
Chang, F.Q., Vis, C.M., Ciptonugroho, W., Bruijnincx, P.C.A., 2021. Recent developments in catalysis with Pickering Emulsions. Green Chem., DOI: 10.1039/D0GC03604H.
Christopher, G.F., Noharuddin, N.,N., Taylor, J.A., Anna, S.L., 2008. Experimental observations of the squeezing-to-dripping transition in T-shaped microfluidic junctions. Phy. Rev. E 78, 036317.
Crossley, S., Faria, J., Shen, M., Resasco, D.E., 2010. Solid nanoparticles that catalyze biofuel upgrade reactions at the water/oil interface. Science. 327, 68-72.
Cubaud, T., Mason, T.G., 2008. Capillary threads and viscous droplets in square microchannels. Phys. Fluids 20, 053302.
de Menech, M., Garstecki, P., Jousse, F., Stone, H.A., 2008. Transition from squeezing to dripping in a microfluidic T-shaped junction. J. Fluid Mech., 595, 141-161.
Fu, T.T., Ma, Y.G., Funfschilling, D., Zhu, C.Y., Li, H.Z., 2010. Squeezing-to-dripping transition for bubble formation in a microfluidic T-junction. Chem. Eng. Sci. 65, 3739-3748.
Fu T.T., Wei L.J., Zhu C.Y., Ma Y.G., 2015. Flow patterns of liquid-liquid two-phase flow in non-Newtonian fluids in rectangular microchannels. Chem. Eng. Process. 91, 114-120.
Garstecki, P., Fuerstman, M.J., Stone, H.A., Whitesides, G.M., 2006. Formation of droplets and bubbles in a microfluidic T-junction—scaling and mechanism of break-up. Lab Chip, 6, 437-446.
Guo, F., Chen, B., 2009. Numerical study on Taylor bubble formation in a micro-channel T-junction using VOF method. Microgravity Sci. Technol. 21, S51-S58.
Husny, J., Cooper-White, J.J., 2006. The effect of elasticity on drop creation in T-shaped microchannels. J. Non-Newtonian Fluid Mech. 137, 121-136.
Jähnisch, K., Hessel, V., Löwe, H., Baerns, M., 2004. Chemistry in microstructured reactors. Angew. Chem. Int. Ed. 43, 406-446.
Jin, N., Yue J., Zhao, Y.C., Lv, H.Y., Wang, C.X., 2020. Experimental study and mass transfer modelling for extractive desulfurization of diesel with ionic liquid in microreactors. Chem. Eng. J. doi.org/10.1016/j.cej.2020.127419.
Kececi, S., Wörner, M., Onea, A., Soyhan H.S., 2009. Recirculation time and liquid

slug mass transfer in co-current upward and downward Taylor flow. Catal. Today 147, S125-S131.
Kim, Y.W., Yoo, J.Y., 2012. Transport of solid particles in microfluidic channels. Opt. Lasers Eng. 50, 87-98.
Kobayashi, J., Mori, Y., Okamoto, K., Akiyama, R., Ueno, M., Kitamori, T., Kobayashi, S., 2004. A microfluidic device for conducting gas-liquid-solid hydrogenation reactions. Science 304, 1305-1308.
Leclerc, A., Philippe, R., Houzelot, V., Schweich, D., de Bellefon, C., 2010. Gas-liquid Taylor flow in square micro-channels: New inlet geometries and interfacial area tuning. Chem. Eng. J. 165, 290-300.
Leclercq, L., Mouret, A., Proust, A., Schmitt, V., Bauduin, P., Aubry, J.M., Nardello-Rataj, V., 2012. Pickering emulsion stabilized by catalytic polyoxometalate nanoparticles: A new effective medium for oxidation reactions. Chem. Eur. J. 18, 14352-14358.
Liedtke, A.K., Bornette, F., Philippe, R., Bellefon, C.D., 2013. Gas-liquid-solid "slurry Taylor" flow: Experimental evaluation through the catalytic hydrogenation of 3-methyl-1-pentyn-3-ol. Chem. Eng. J. 227, 174-181.
Liedtke, A.K., Scheiff, F., Bornette, F., Philippe, R.G., Agar, D.W., Bellefon, C.D., 2015. Liquid-solid mass transfer for microchannel suspension catalysis in gas-liquid and liquid-liquid segmented flow. Ind. Eng. Chem. Res. 54, 4699-4708.
Liu, H., Wang, C.Y., Zou, S.W., Wei, Z.J., Tong, Z., 2012. Facile fabrication of polystyrene/halloysite nanotube microspheres with core-shell structure via Pickering suspension polymerization. Polymer Bulletin 69, 765-777.
Liu, W., Zhao, Y.J., Zeng, C.F., Wang, C.Q., Serra, C.A., Zhang, L.X.,2017. Microfluidic preparation of yolk/shell ZIF-8/alginate hybrid microcapsules from Pickering emulsion. Chem. Eng. J. 307, 408-417.
Márquez, N., Moulijn, J., Makkee, M., Kreutzer, M.T., Castaño, P., 2019. Tailoring the multiphase flow pattern of gas and liquid through micro-packed bed of pillars. React. Chem. Eng. 4, 838-851.
Meng, Y., Sun, W.X., Yang, H., Wang, W., Jin, N., Zhang, X.L., Zhao, Y.C., Lv, H.Y., 2020. Fine tuning of surface properties of SiO_2 nanoparticles for the regulation of Pickering emulsions. Colloid. Surface. A. 592, 124603.
Munirathinam, R., Huskens, J., Verboom, W., 2015. Supported catalysis in continuous-flow microreactors. Adv. Synth. Catal. 357, 1093-1123.
Pan, D.W., Liu, M.F., Li, F., Chen, Q., Liu, X.D., Liu, Y.Y., Zhang, Z.W., Huang, W.X., Li, B., 2018. Formation mechanisms of solid in water in oil compound droplets in a horizontal T-junction device. Chem. Eng. Sci. 176, 254-263.
Qi, L., Luo, Z., Lu, X., Facile synthesis of starch-based nanoparticle stabilized Pickering emulsion: its pH-responsive behavior and application for recyclable catalysis. Green Chem. 2018, 20:1538-50.
Shao, N., Salman, W., Gavriilidis, A., Angeli, P., 2008. CFD simulations of the effect of inlet conditions on Taylor flow formation. Int. J. Heat Fluid Flow 29, 1603-1611.
Shen, M., Resasco, D.E., 2009. Emulsions stabilized by carbon nanotube-silica nanohybrids. Langmuir 25, 10843-10851.
Su, Y.H., Chen, G.W., Yuan, Q., 2012. Influence of hydrodynamics on liquid mixing during Taylor flow in a microchannel. AIChE J. 58, 1660-1670.
Tanimu, A., Jaenicke, S., Alhooshani, K., 2017. Heterogeneous catalysis in continuous flow microreactors: A review of methods and applications. Chem. Eng. J. 327,

792-821.
Thorsen, T., Roberts, R.W., Arnold, F.H., Quake, S.R., 2001. Dynamic pattern formation in a vesicle-generating microfluidic device. Phy. Rev. Lett. 86, 4163-4166.
Tice, J.D., Song, H., Lyon, A.D., Ismagilov, R.F., 2003. Formation of droplets and mixing in multiphase microfluidics at low values of the Reynolds and the capillary numbers. Langmuir 19, 9127-9133.
Tidona, B., Desportes, S., Altheimer, M., Ninck, K., von Rohr, P.R., 2012. Liquid-to-particle mass transfer in a micro packed bed reactor. Int. J. Heat Mass Transfer 55, 522-530.
Tsaoulidis, D., Dore, V., Angeli, P., Plechkova, N.V., Seddon, K.R., 2013. Flow patterns and pressure drop of ionic liquid-water two-phase flows in microchannels. Int. J. Multiphase Flow 54, 1-10.
Vadivukkarasan, M., Dhivyaraja, K., Panchagnula, M.V., 2020. Breakup morphology of expelled respiratory liquid: From the perspective of hydrodynamic instabilities. Phys. Fluids 32, 094101.
van Steijn, V., Kreutzer, M.T., Kleijn, C.R., 2007. μ-PIV study of the formation of segmented flow in microfluidic T-junctions. Chem. Eng. Sci. 62, 7505-7514.
Vis, C.M., Nieuwelink, A.E., Weckhuysen, B.M., Bruijnincx, P.C.A., 2020. Continuous flow Pickering emulsion catalysis in droplet microfluidics studied with in situ Raman microscopy. Chem. Eur. J. 26, 15099-15102.
Wang, H. Shen, Q.y., Zhu, C.Y., Ma, Y.G., Fu. T.T., 2021. Formation and uniformity of bubbles in highly viscous fluids in symmetric parallel microchannels. Chem. Eng. Sci. 230, 116166.
Wu, J., Ma G.H., 2016. Recent studies of Pickering emulsions: particles make the difference. Small 12, 4633-4648.
Wang, K., Lv, Y.C., Yang, L., Luo, G.S., 2013. Microdroplet coalescences at microchannel junctions with different collision angles. AIChE J. 59, 643-649.
Wang, Z.P., van Oers, M.C.M., Rutjes, F.P.J.T., van Hest, J.C.M., 2012. Polymersome colloidosomes for enzyme catalysis in a biphasic system. Angew. Chem. Int. Ed. 124, 10904-10908.
Xiao, F., Dianat, M., McGuirk, J.J., 2016. A robust interface method for drop formation and breakup simulation at high density ratio using an extrapolated liquid velocity. Comput. Fluids 136, 402-420.
Xiong, R.Q., Bai, M., Chung, J.N., 2007. Formation of bubbles in a simple co-flowing micro-channel. J. Micromech. Microeng. 17, 1002-1011.
Xu, J.H., Li, S.W., Tan, J., Luo, G.S., 2008. Correlations of droplet formation in T-junction microfluidic devices: from squeezing to dripping. Microfluid. Nanofluid. 5, 711-717.
Yagodnitsyna, A.A., Kovalev, V.A., Bilsky, V.A., 2016. Flow patterns of immiscible liquid-liquid flow in a rectangular microchannel with T-junction. Chem. Eng. J. 303, 547-554.
Yang, H.Q., Fu, L.M., Wei, L.J., Liang, J.F., Binks, B.P., 2015. Compartmentalization of incompatible reagents within Pickering emulsion droplets for one-pot cascade reactions. J. Am. Chem. Soc. 137, 1362-1371.
Yang, X.M., Wang, X.N., Qiu, J.S., 2010. Aerobic oxidation of alcohols over carbon nanotube-supported Ru catalysts assembled at the interfaces of emulsion droplets. Appl. Catal. A-Gen. 382, 131-137.
Yao, C.Q., Zhao, Y.C., Chen, G.W., 2018. Multiphase processes with ionic liquids in microreactors: hydrodynamics, mass transfer and applications. Chem. Eng. Sci.

189, 340-359.
Yue, J., 2017. Multiphase flow processing in microreactors combined with heterogeneous catalysis for efficient and sustainable chemical synthesis. Catal. Today 308, 3-19.
Zaloha, P., Kristal, J., Jiricny, V., Völkel, N., Xuereb, C., Aubin, J., 2012. Characteristics of liquid slugs in gas-liquid Taylor flow in microchannels. Chem. Eng. Sci. 68, 640-649.
Zhang, M., Wei, L., Chen, H., Du, Z., Binks, B. P., Yang, H., 2016. Compartmentalized droplets for continuous flow liquid-liquid interface catalysis. J. Am. Chem. Soc. 138, 10173-10183.
Zhang, Q., Liu, H.C., Zhao, S.N., Yao, C.Q., Chen, G.W., 2019. Hydrodynamics and mass transfer characteristics of liquid-liquid slug flow in microchannels: The effects of temperature, fluid properties and channel size. Chem. Eng. J. 358, 794-805.
Zhang, Q.D., Zhu, C.Y., Du, W., Liu, C., Fu, T.T., Ma, Y.G., Li, H.Z., 2018. Formation dynamics of elastic droplets in a microfluidic T-junction. Chem. Eng. Res. Des. 139, 188-196.
Zhao, Y.C., Chen, G.W., Yuan, Q., 2006. Liquid-liquid two-phase flow patterns in a rectangular microchannel. AIChE J. 52, 4052-4060.
Zhao, Y.C., Chen, G.W., Ye, C.B., Yuan, Q., 2013. Gas-liquid two-phase flow in microchannel at elevated pressure. Chem. Eng. Sci. 87, 122-132.